Reconstructing past hydrology of eastern Canadian boreal catchments using clastic varved sediments and hydro-climatic modelling: 160 years of fluvial inflows

Antoine Gagnon-Poiré[1-2-3], Pierre Brigode[4], Pierre Francus[1-2-3-5], David Fortin[1-6], Patrick Lajeunesse[7], Hugues Dorion[7] and Annie-Pier Trottier[7]

[1] *Institut national de la recherche scientifique, Centre Eau Terre Environnement, Québec, QC, Canada.*
[2] *GEOTOP, Research Centre on the Dynamics of the Earth System, Montréal, QC, Canada.*
[3] *Centre d'études nordiques, Québec, QC, Canada.*
[4] *Université Côte d'Azur, CNRS, OCA, IRD, Géoazur, Nice, France.*
[5] *Canada Research Chair in Environmental sedimentology.*
[6] *Department of Geography and Planning, University of Saskatchewan, Saskatoon, SK, Canada.*
[7] *Département de géographie, Université Laval, Québec, QC, Canada.*

Corresponding author: Antoine Gagnon-Poiré (Antoine.Gagnon-Poire@ete.inrs.ca)

Abstract

Analysis of short sediment cores collected in Grand Lake, Labrador, revealed that this lake is an excellent candidate for the preservation of laminated sediments record. The great depth of Grand Lake, the availability of fine sediments along its tributaries, and its important seasonal river inflow have favoured the formation of a 160 years-long clastic varved sequence. Each varve represents one hydrological year. Varve formation is mainly related to spring discharge conditions with contributions from summer and autumn rainfall events. The statistically significant relation between varve parameters and the Naskaupi River discharge observations provided the opportunity to develop local hydrological reconstructions beyond the instrumental period. The combined detrital layer thickness and the particle size (99th percentile) series extracted from each varve yield the strongest correlations with instrumental data ($r = 0.68$ and 0.75) and have been used to reconstruct Naskaupi River mean and maximum annual discharges, respectively, over the 1856-2016 period. The reconstructed Q-mean series suggest that high Q-mean years occurred during the 1920-1960 period and a slight decrease in Q-mean takes place during the second half of the 20th century. Independent reconstructions based on rainfall-runoff modelling of the watershed from historical reanalysis of global geopotential height fields display a significant correlation with the reconstructed Naskaupi River discharge based on varve physical parameters. The Grand Lake varved sequence contains a regional hydrological signal, as suggested by the statistically significant relation between the combined detrital layer thickness series and the observed Labrador region Q-mean series extracted from five watersheds of different sizes.

1. Introduction

Climate changes caused by rising concentrations of greenhouse gases can alter hydro-climatic conditions on inter- and intra-regional scales (Linderholm et al., 2018; Ljungqvist et al., 2016; Stocker et al., 2013). Hydropower, which is considered as a key renewable energy source to mitigate global warming, has strong sensitivity to changes in hydrological regime especially in vulnerable northern regions (Cherry et al., 2017). Therefore, a clear understanding of the regional impacts that recent climate change combined with natural climate variability can have on river discharge and hydroelectric production is needed.

However, the lack of instrumental records and the uncertainty related to hydroclimate variability projections (Collins et al., 2013) are obstacles to sustainable management of these water resources.

The Labrador region in eastern Canada is a critical area for hydropower generation, hosting the Churchill River hydroelectric project, one of the largest hydropower systems in the world. Average annual streamflow has been varying in eastern Canada during the last fifty years, with higher river discharges from 1970 to 1979 and 1990 to 2007, and lower discharges from 1980 to 1989 (Mortsch et al., 2015; Déry et al., 2009; Jandhyala et al., 2009; Sveinsson et al., 2008; Zhang et al. 2001). These changes in streamflow represent a significant economic challenge for the long-term management of hydropower generation. The few decades of available instrumental observations (<60 years) and their low spatial coverage are not sufficient to allow a robust analysis of multi-decadal hydrological variability.

The study of multi-decadal hydrological variability requires long instrumental records (>100 years), but such long-time series are non-existent for the Labrador region. Recently, rainfall-runoff modelling approaches have been used to expand instrumental streamflow datasets, using long-term climatic reanalysis as inputs. Rainfall-runoff modelling was used by Brigode et al. (2016) to reconstruct daily streamflow series over the 1881–2011 period in northern Québec. Nevertheless, this type of method suffers from the limited observations in order to evaluate and validate the reconstructed hydro-climatic temporal series. The deficiency of observations led to the exploration of various natural archives for reconstructing past hydro-climatic conditions. Long hydro-climatic series based on natural proxies in eastern Canada are rare, limited to a tree ring (Boucher et al., 2017; Begin et al., 2015; Naulier et al., 2015; Nicault et al., 2014; Boucher et al., 2011; Begin et al., 2007; D'Arrigo et al., 2003) and pollen datasets (Viau et al., 2009) and mainly focused on temperature reconstructions. Reconstructing river hydrological series using dendrological analysis is complex in the boreal region due to the indirect relation between tree ring indicators and streamflow. One study has reconstructed streamflow variations over the last two centuries in Labrador based on tree-ring isotopes series (Dinis et al., 2019). Still, the

spatial coverage of palaeohydrological records from independent proxies must be increased in this region. In this perspective, annually laminated sediments composed of minerogenic particles (clastic varves) formed when seasonal runoff carrying suspended sediment enters a lake (Sturm, 1979) have the potential to produce long paleohydrological series. The direct relationship between clastic varves and hydrological conditions makes this type of varve a specific and powerful proxy for streamflow reconstructions. Clastic varves can provide, in favourable settings, annually to seasonally resolved information about downstream sediment transport from catchment area into lake basin depending on regional hydro-climatic conditions (Lamoureux, 2000; Lamoureux et al., 2006; Tomkins et al., 2010; Cuven et al., 2011; Kaufman et al., 2011; Schillereff et al., 2014; Amann et al., 2015; Heideman et al., 2015; Zolitschka et al., 2015; Saarni et al., 2016; Czymzik et al., 2018).

Preliminary analysis of short sediment cores collected in Grand Lake, central Labrador, revealed that this lake is an excellent candidate for the preservation of recent fluvial clastic laminated sediment record (Zolitschka et al., 2015). The objectives of this paper are to: (1) Confirm the annual character of the laminations record; (2) Establish the relation between the physical parameters of laminations and local hydrological conditions to examine the potential proxy for hydrological reconstructions; (3) Reconstruct the hydrology of the last 160 years and compare its similarities and differences with Brigode et al. (2016) rainfall-runoff modelling over the 1880-2011 period; and (4) Determine if there is a Labrador regional streamflow signal recorded in Grand Lake laminated sediments.

2. Regional setting

Grand Lake is a 245-m-deep (Trottier et al., 2020) elongated (60-km-long) fjord-lake located in a valley connected to the Lake Melville graben in central Labrador (53°41'25.58"N, 60°32'6.53"O, ~15 m above sea level) (Fig. 1). The region is part of the Grenville structural province and is dominated by Precambrian granite, gneiss and acidic intrusive rocks. Grand Lake watershed deglaciation began after ~8.2 cal ka BP (Trottier et al., 2020). During deglaciation, marine limit reached an elevation of 120-150 m above modern sea level and invaded further upstream in the modern fluvial valleys that are connected to the lake (Fizthugh, 1973). This former glaciomarine/marine sedimentary fjord

basin has been glacio-isostatically uplifted and isolated by a morainic sill to become a deep fjord-lake (Trottier et al., 2020). The regional geomorphology is characterized by glacially sculpted bedrock exposures, glacial deposits consisting of till plateaus of various elevations, glacial lineations, drumlins, kames, eskers and raised beaches (Fulton 1992). Podzolic soils dominate, with inclusions of brunisols and wetlands.

Grand Lake is located in the High Boreal Forest ecoregion, one of the most temperate climates in Labrador, hosting mixed forests dominated by productive, closed stands of Abies balsamea, Picea mariana, Betula papyrifera, and Populus tremuloides (Riley et al., 2013). This region is influenced by temperate continental (westerly and southwesterly winds) and maritime (Labrador Current) conditions with cool humid summers (JJA) (~8.5 °C) and cold winters (DJFM) (~-13 °C). The Grand Lake watershed extends upstream over the low subarctic Nipishish-Goose ecoregion, a broad bedrock plateau (<700 m.a.s.l.) located on the west flank of the Lake Melville lowlands. Lichen-rich Picea woodlands with open canopies predominate. With cooler summers and longer cold winters, this area is slightly influenced by the Labrador Sea. Mean annual precipitation in the study region ranges from 800 mm to 1 000 mm, with 400 cm to 500 cm of snowfall. The regional hydrological regime typically exhibits winter low flow and spring freshet, followed by summer flow recession (Fig. 2). Snowmelt in Grand Lake region takes place from April to June (AMJ).

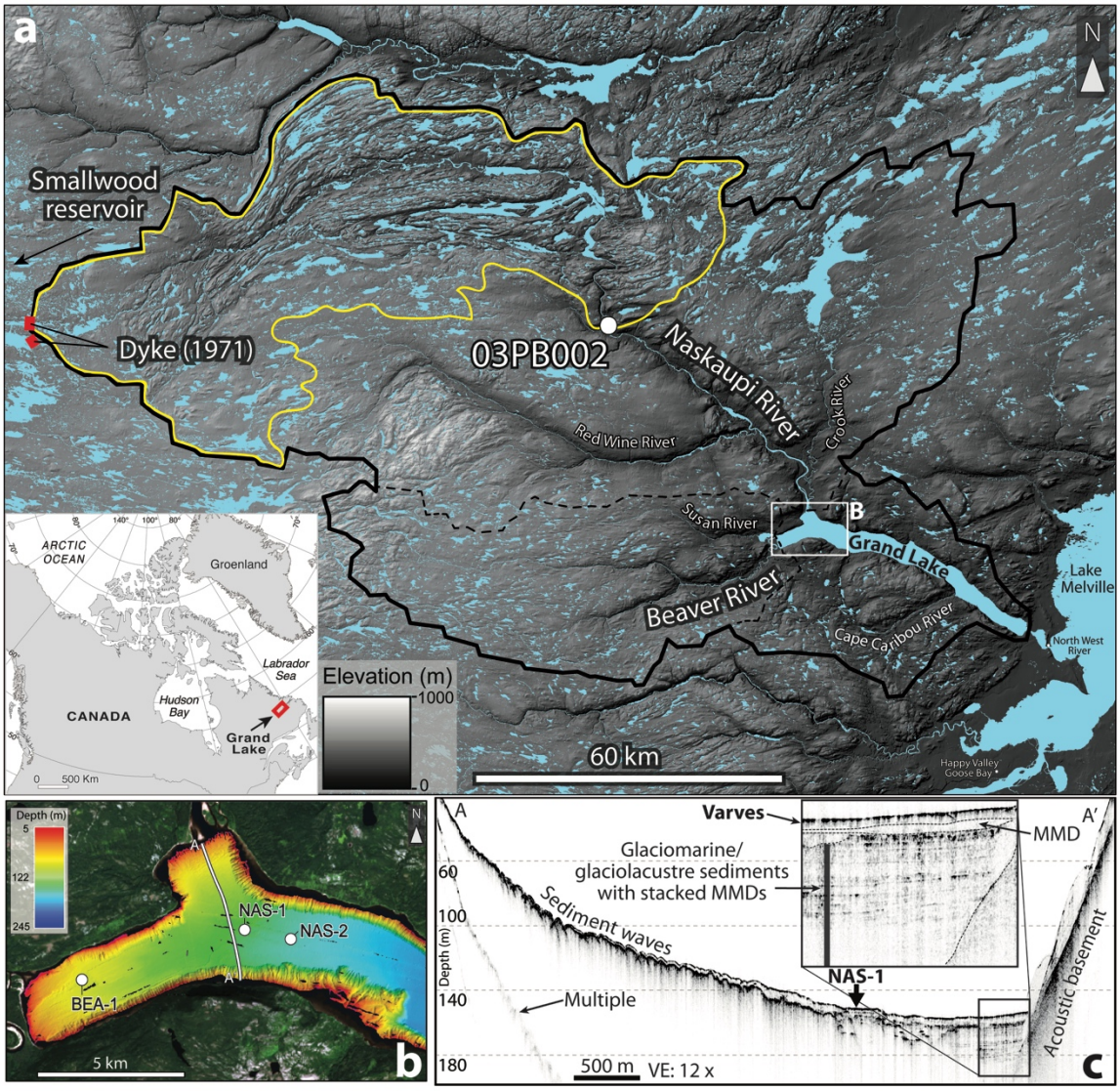

Figure 1. (A) Location of Grand Lake watershed (black line) and its principal tributaries. The Naskaupi River hydrometric station (03PB002: white dot) covering an area of 4480 km^2 (yellow line). Location of the dykes constructed in 1971 to divert water from the Naskaupi River to the Smallwood reservoir hydroelectric system are also shown by the red bars. (B) High-resolution swath bathymetry (1-m resolution) of Grand Lake (Trottier et al., 2020) coupled with a Landsat image (USGS) and core site locations. The white line indicates the location of (C) a typical 3.5 kHz subbottom profile of the Naskaupi River delta (A-A') showing the approximate location of core NAS-1. MMD: mass-movement deposit.

The main tributary of Grand Lake is the Naskaupi River located at the lake head (Fig. 1a). The downstream part of the Naskaupi River is fed by the Red Wine and the Crook rivers. The Beaver River is the secondary tributary of Grand Lake. Naskaupi and Beaver rivers structural valleys that connect to the Grand Lake Basin have a well-developed fluvial plain and a generally sinuous course that remobilize former deltaic systems and terraces composed of glaciomarine, marine, fluvio-glacial, lacustrine and modern fluvial deposits.

Upstream river terraces show mass movement scarps and are affected by gully and aeolian activity. Grand Lake flows into a small tidal lake (Little Lake) and subsequently towards Lake Melville. On 28 April 1971, by closing a system of dykes, the headwaters of Naskaupi River watershed (Lake Michikamau) were diverted into the Churchill River hydropower development (Fig. 1a). This diversion has reduced the drainage area of the Naskaupi River from 23 310 km^2 to 12 691 km^2 (Anderson, 1985).

Hydroacoustic data were collected in Grand Lake in 2016 (Trottier et al., 2020). The swath bathymetric imagery and 3.5 kHz subbottom profile show that the prodelta slopes present well-defined sediment waves at the Naskaupi River mouth (Trottier et al., 2020; Fig. 1b). The upper acoustic unit is composed of a high amplitude acoustic surface changing into low amplitude acoustic parallel reflections (Fig. 1c), a type of acoustic facies which can be associated with successive sedimentary layers of contrasting particle sizes (Gilbert and Desloges, 2012).

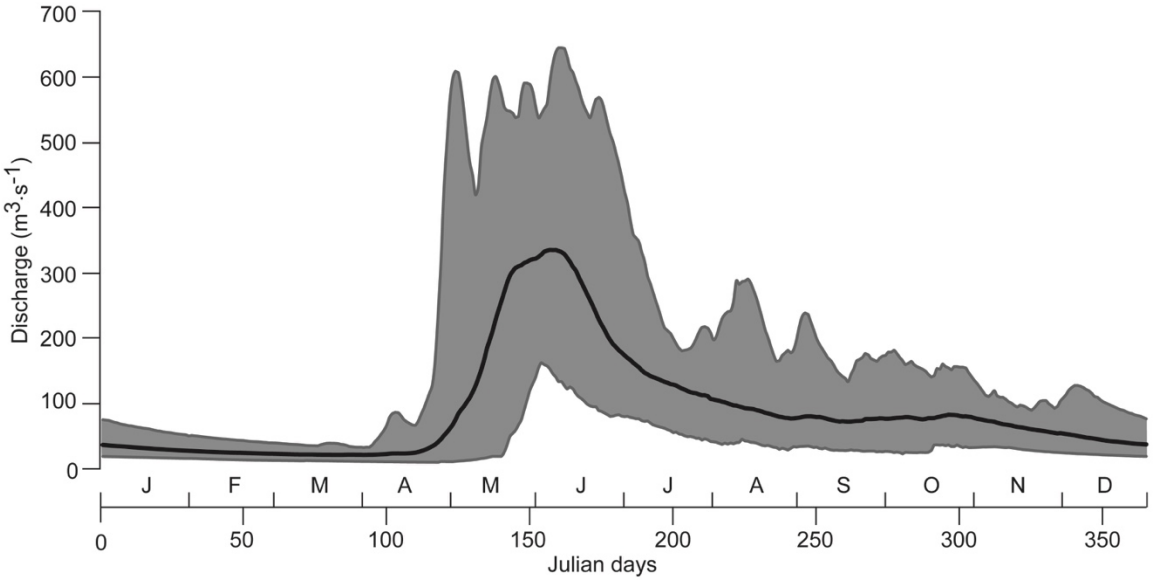

Figure 2. Observed mean daily discharges of the Naskaupi River (hydrometric station 03PB002) for the 1978-2012 period (black line). The gray zone represents the minimum and maximum observed discharges.

3. Methods

3.1 Sediment coring and processing

Four short sediment cores (BEA-1, NAS-1A, NAS-1B and NAS-2) were collected using a UWITEC percussion corer in March 2017 deployed from the lake ice cover. These cores were collected in undisturbed areas according to the swath bathymetry and subbottom profiling data (Trottier et al., 2020). Core BEA-1 was collected in the axis of the Beaver River at a depth of 93 m. Core NAS-1 was collected in the axis of the Naskaupi River at a depth of 146 m (Fig. 1b). Site BEA-1 and NAS-1 were collected from locations sharing relative similarities: at the distal frontal slope of the Beaver and Naskaupi river deltas (fig. 1c). Site NAS-2 was collected away from the Naskaupi River delta, 176 m deep at the beginning of the deep lake basin. Sites NAS-2 is mainly fed by sediments from the Naskaupi River, but is also in a distal position to the Beaver River. Duplicate cores of different lengths have been retrieved at each site to maximize undisturbed sediment recovery. Following the extraction of each core, wet floral foam was gently inserted through the top of the filled coring tube and slowly pushed towards the sediment surface to seal and preserve the sediment-water interface. A plastic cap was then installed on top of the foam to secure its position in contact with the intact sediment surface and avoid disturbance during transport of the cores. The cores were scanned using a Siemens SOMATOM Definition AS+ 128 medical CT-Scanner at the multidisciplinary laboratory of CT-scan for non-medical use of the Institut National de la Recherche Scientifique - Eau Terre Environnement (INRS-ETE). The CT-scan images allowed the identification of sedimentary structures (i.e., laminated facies, perturbation and hiatus). Expressed as CT-numbers or Hounsfield units (HU), X-Ray attenuation is a function of density and the effective atomic number, and hence sensitive to contrasts in mineralogy, grain size and sediment porosity (St-Onge et al., 2007). CT-numbers were extracted at a resolution of 0.06 cm using the ImageJ software 2.0.0 (imagej.net). The cores were then opened, described and photographed with a high-resolution line-scan camera mounted on an ITRAX core scanner (RGB colour images; 50 µm-pixel size) at INRS-ETE. Geochemical non-destructive X-Ray Fluorescence (XRF) analysis was performed on the core half (30 kV and 30 mA). XRF elements profiles were used to visualize the structures and boundaries

of the laminations and estimate particle size variability in sediment cores (Kylander et al., 2011; Cuven et al., 2010; Croudace et al., 2006). Elements were normalized by the total of count (cps) for each spectrum. Continuous XRF measurements were also carried out on overlapping impregnated sediment blocks in order to superpose element relative intensity profiles on thin-sections.

3.2 Chronology and thickness measurement

Surface sediments from cores BEA-1 and NAS-1A were dated with ^{137}Cs method (Appleby and Oldfield 1978) using a high-resolution germanium diode gamma detector and multichannel analyzer gamma counter. ^{137}Cs activity was used to identify sediment deposited during 1963-1964 peak of nuclear tests and validate the annual character of the layers. A sampling interval of 2 cm was used to approximately identify the depth at which the ^{137}Cs peaks were located. Subsequently, a sampling interval of ± 0.5 cm was used to sample each lamination for the period 1961-1965 to determine the exact ^{137}Cs peak location (1963-1964). In order to establish a chronology for each core, detailed laminations counts were executed on CT-scan images and high-resolution photographs using ImageJ 2.0.0 and Adobe Illustrator CC softwares (Francus et al., 2002). As all of the core surface has been well preserved, the first complete lamination below the sediment surface was considered to represent the topmost year (i.e., 2016 CE). Chronology on each core was confirmed by cross-correlation between thick laminations selected as distinctive marker layers along the different sediment sequences (A to M; Fig. 4).

Thin-sections of sediments were sampled from cores BEA-1 (1856-2016), NAS-1A (1953-2016), NAS-1B (1856-1952) and NAS-2 (1968-2016) (see Fig. 4 for thin-section location) following Francus and Asikainen (2001) and Lamoureux (1994). Digital images of the thin-sections were obtained using a transparency flatbed scanner at 2400 dpi resolution (1 pixel = 10.6 µm) in plain light and were used to characterize lamination substructure. Lamination counts and thickness measurements using a thin-section image analysis software developed at INRS-ETE (Francus and Nobert 2007) were performed to duplicate and validate previous chronologies established on CT-Scan images and high-resolution photographs. Two counts were made from thin-section by the same observer (AGP). Total Varve

227 Thickness (TVT) and Detrital Layer Thickness (DLT) of each year of sedimentation were
228 measured from images of thin-sections. Lamination counts made on CT-scan images, high-
229 resolution photographs and thin-sections are identical while TVT measurements show
230 negligible difference ($R^2 = 0.96$; $p < 0.05$). The thickness measurements made from CT-
231 scan images and high-resolution photographs have been used to prolong the TVT series of
232 core NAS-2 from 1968 back to 1856. Continuous TVT measurements allowed the
233 establishment of high-resolution age-depth models for each site.

234 **3.3 Image and particle size analysis**

235 Using custom-made Image Analysis software (Francus and Nobert, 2007), regions of
236 interest (ROIs) were selected on the thin-section images. The software then automatically
237 yielded scanning electron microscope (SEM) images of the ROIs using a Zeiss Evo 50
238 SEM in backscattered electron (BSE) mode. Eight-bit greyscale BSE images with a
239 resolution of 1024 x 768 pixels were obtained with an accelerating voltage of 20 kV, a tilt
240 angle of 6.1 and an 8.5 mm working distance with a pixel size of 1 µm. BSE images were
241 processed to obtain black and white images where clastic grains (>3.5 µm) and clay matrix
242 appeared black and white respectively (Francus, 1998).
243
244 Each sedimentary particle (an average of 2 225 particles per image) was measured
245 according to the methodology used by Lapointe et al. (2012), Francus et al. (2002) and
246 Francus and Karabanov (2000) in order to calculate particle size distribution on each ROI
247 image. Due to the thickness of the laminations, results from several ROI images were
248 merged to obtain measurements for each year of sedimentation, with an average of 4
249 images per lamination. Only clastic facies related to spring and summer discharges were
250 used for particle size analysis in order to exclude ice-rafted debris (µm to mm scale)
251 observed in the early spring layers (see Fig. 5 for details). The 99th percentile ($P99D_0$) of
252 the particle size distribution for each detrital layer was obtained from thin-sections
253 (Francus, 1998) for the last 160 years (1856-2016) for core BEA-1 and NAS-1, and for the
254 last 47 years (1968-2016) for core NAS-2, from 795, 717 and 132 BSE images respectively
255 (Fig. 4).
256

3.4 Hydrological variables

Hydrological variables (Tab.1) were calculated from the time series of daily discharges recorded by the Naskaupi River hydrometric station over the 1978-2011 period (missing data from the years 1996, 1997 and 1998).

Table 1. Hydrological variables used in this paper

Hydrological variable	Unit	Description
Q-max	m^3/s	Annual maximum of daily discharges
Q-mean	m^3/s	Mean annual discharge
Q-max-Jd	Julian days	Julian day at which the discharge reaches its maximum annual value
Rise-Time	Days	Number of days between the minimum winter flow and the maximum spring flow
Nb-Days-SupQ80	Days	Number of days with discharge greater than the 80^{th} daily percentile
Q-nival	mm	Nival runoff (April, May, June, July)

The Naskaupi River hydrological variables have been compared with four other hydrometric station data available around the study region (Fig. 3a, Tab. 2), which are devoid of anthropogenic perturbations. Q-mean series from the five stations have been normalized for the common 1979–2011 period and averaged, to produce a Labrador region mean annual discharge series. This allows to extend instrumental data series for the period 1969 to 2011, and fill in data for the missing years. The Labrador hydrometric station data used in this study come from a Government of Canada website (https://wateroffice.ec.gc.ca 05/2018).

Table 2. Description of hydrometric stations used in this study

Hydrometric station	ID	Area (km^2)	Location (N,W)	Recording period
Ugjoktok River	03NF001	7570	55° 14' 02", 61° 18' 06"	1979-2011
Naskaupi River	03PB002	4480	54° 07' 54", 61° 25' 36"	1978-2011
Minipi River	03OE003	2330	52° 36' 45", 61° 11' 07"	1979-2011
Little Mecatina River	02XA003	4540	52° 13' 47", 61° 19' 01"	1979-2011
Eagle River	03QC001	10 900	53° 32' 03", 57° 29' 37"	1969-2011

3.5 Varve physical parameters and hydrological variables

A simple linear regression model was used to fit the DLT and $P99D_0$ series with local (1978-2011) and regional (1969–2011) instrumental series and reconstructed hydrological variables (Q-mean, Q-max) back to 1856. Model calibration was performed using a

281 twofold cross-validation technique over the instrumental period. Root mean squared errors
282 (RMSE) and coefficient of determination (R^2) were calculated for calibration periods,
283 while average reduction of error (RE) and average coefficient of efficiency (CE) were
284 calculated to evaluate reconstruction skills (Briffa et al. 1988, Cook et al., 1999). The RE
285 and CE of the verification periods must be > 0 to validate the model skills. Statistical
286 analysis was realized using the treeclim package (Zang and Biondi, 2015) in the R-project
287 environment (R Core Team, 2019, http://www.r-project.org/).
288

289 **3.6 Hydro-climatic reconstruction based on rainfall-runoff modelling**

290 The applied reconstruction method is based on rainfall-runoff modelling. Firstly, it aims at
291 producing, for the Naskaupi River hydrometric station catchment (Fig. 1a), daily climatic
292 time series using a historical reanalysis of global geopotential height fields extracted over
293 the studied region for a given time period (here 1880-2011). Secondly, the produced
294 climatic series are used as inputs to a rainfall–runoff model previously calibrated on the
295 studied catchment in order to obtain daily streamflow time series. The reconstruction
296 method is fully described in Brigode et al. (2016) and was recently applied over
297 southeastern Canada catchments in Dinis et al. (2019). It is summarized in the following
298 paragraphs.
299

300 The available observed hydro-climatic series for the Naskaupi River hydrometric station
301 catchment have been aggregated at the catchment scale. Climatic series (daily air
302 temperature and precipitation) have been extracted from the CANOPEX dataset (Arsenault
303 et al., 2016), built using Environment Canada weather stations and Thiessen polygons to
304 calculate climatic series at the catchment scale. Daily air temperature series have been used
305 for calculating daily potential evapotranspiration at the catchment scale, using the Oudin
306 et al. (2005) formula designed for rainfall-runoff modelling.
307

308 These daily series have been used for calibrating the GR4J rainfall-runoff model (Perrin et
309 al., 2003) and its snow accumulation and melting module, CemaNeige (Valéry et al.,
310 2014a), using the airGR package (Coron et al., 2017). This combination of GR4J and
311 CemaNeige (hereafter denoted CemaNeigeGR4J) has been recently applied over eastern

Canada catchments and showed good modelling performances (e.g., Seiller et al., 2012; Valéry et al., 2014b, Brigode et al., 2016). CemaNeigeGR4J has been calibrated on the recorded period of the Naskaupi River hydrometric station catchment using the Kling and Gupta efficiency criterion (Gupta et al., 2009) as objective function.

Then, the observed climatic series have been resampled over the 1880-2011 period, based on both season and similarity of geopotential height fields (Kuentz et al., 2015). The resampling is performed by calculating Teweles and Wobus (1954) distances between four geopotential height fields: (i) 1000 hPa at 0 h, (ii) 1000 hPa at 24 h, (iii) 500 hPa at 0 h, and (iv) 500 hPa at 24 h. The NOAA 20th Century Reanalysis ensemble (Compo et al., 2011, hereafter denoted 20CR) has been used as a source of geopotential height fields (Fig. 3b).

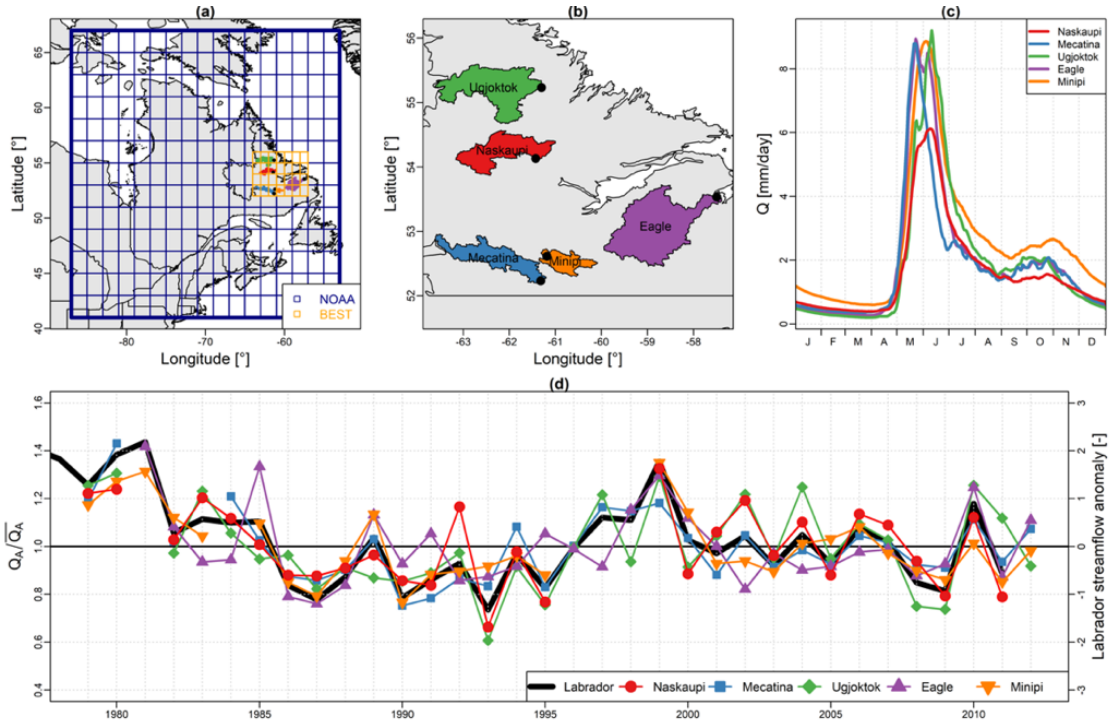

Figure 3. (a) Dataset used for the hydro-climatic reconstruction based on rainfall-runoff modelling: the extension of the 20CR grid used is shown in blue, while the BEST grid used is highlighted in orange. (b) Spatial distribution of hydrometric stations used in this study (black dots) and their catchment area. (c) Observed mean daily discharges of each hydrometric station for the 1978-2012 period. (d) Labrador streamflow anomaly and the Labrador region mean annual discharge series (thick black line).

As in Brigode et al. (2016), the resampled series of air temperature have been corrected at the catchment scale using a regression model calibrated with the Berkeley Earth Surface Temperature analysis (Rohde et al., 2013, hereafter denoted BEST). BEST is a gridded air temperature product starting in 1880 at the daily timestep (Fig. 3b).

Finally, the daily climatic series are used as inputs to the CemaNeigeGR4J model in order to obtain daily streamflow time series on the same 1880-2011 period. Thus, the outputs of the hydro-climatic reconstruction are an ensemble of daily meteorological series (air temperature, potential evapotranspiration and precipitation) and an ensemble of daily streamflow series.

4. Results

4.1 Lamination characterization

Sediment retrieved at the head of Grand Lake (Fig. 4), consist of dark grayish to dark yellowish brown (Munsell colour: 10YR-4/2 to 10YR-4/4) laminated minerogenic material, interpreted as clastic lamination of fluvial origin. Lamination structure can be divided in 3 seasonal layers (Fig. 5) based on their stratigraphic position and microfacies. Annual sedimentation starts with a layer composed of silt and clay sediment matrix which sometimes contains ice-rafted debris (μm to mm scale) interpreted as an early spring layer. The major lamination component is a spring and summer/autumn detrital layer. Its thick basal part is mostly poorly sorted, graded and composed of coarse minerogenic grains comprising fine sand and silts (< 150 μm) with some redeposited cohesive sediment clasts eroded from the underlying early spring layer. This detrital layer has a sharp lower boundary. The upper part of the detrital layer consists of a finer detrital grain matrix containing thin visually coarser intercalated sub-layers in ~75% of the laminations. The allochthonous lithoclastic materials which compose the detrital layers are associated with higher density values (Fig. 4) and an increase in the relative intensity of elements Sr and Ca (Zolitschka et al., 2015). Few organic debris and charcoal fragments are observed throughout the detrital layers. The third topmost lamination layer is formed by a fine to medium silty layer with abundant clay rich in Fe and interpreted as an autumn and winter layer, also known as a clay cap (Zolitschka et al., 2015). The Fe peak values in autumn and

winter layers, are hence used to determine the upper lamination boundary (Fig. 4) (Zolitschka et al., 2015) as previously performed in other varved sequences (Cuven et al., 2010; Saarni et al., 2016).

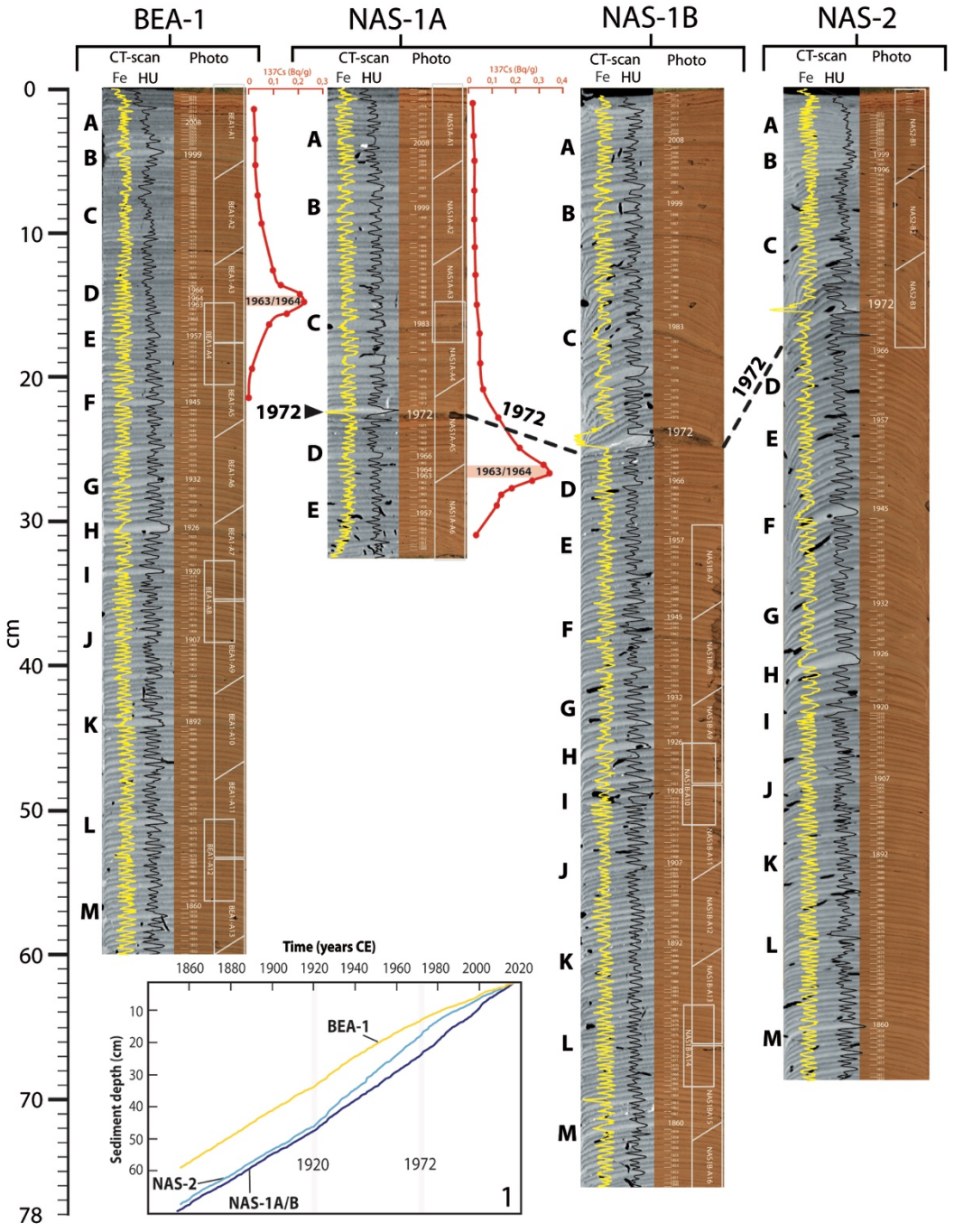

Figure 4. Varve counts made on (left) CT-scan and (right) high resolution images from core BEA-1, NAS-1A/B and NAS-2. Distinctive marker layers are identified by letters A to M. The 1972 marker layer is outlined by the thick dark gray line. Fe relative intensity and density (HU) profile represented by the yellow and black line respectively, show rhythmic laminations. The activity profile of ^{137}Cs in core BEA-1, NAS-1A is shown by the red line. Approximate thin-section locations are outlined by white boxes. The age-depth model of the 3 cores is also presented (Box. 1). See Fig. 1b for core locations.

The lamination deposited in 1972 from sites in the axis of the Naskaupi River (NAS-1; Fig. 5b and NAS-2; Fig. 4), present a thick (8.2 mm) and coarse (67.8 µm) detrital layer composed of very fine sandy and very coarse silt (Fig. 5b) representing the highest particle size measured in all sequences. Furthermore, there is a difference in lamination physical parameters and microfacies deposited before and after the 1972 marker bed, especially in core NAS-1, the proximal site from the Naskaupi River mouth. Laminations deposited prior 1972 have a well-developed substructure relatively constant among each annual lamination (Fig. 5b). The early spring layer of the pre-1972 laminations is thicker and more clearly visible. Conversely, the detrital layer of laminations post-1972 is thicker, while the early spring layer is more difficult to discern and contributes less to the TVT (Fig. 5a). The mean contribution of the early spring layer and autumn and winter layer to the total lamination thickness is 35% for the pre- and 52% for the post-1972 intervals. The early spring layer in lamination post-1971 from sites NAS-1 and NAS-2 no longer contains isolated coarse debris. The changes in lamination facies are less noticeable in core NAS-2, which was sampled further away from the Naskaupi River mouth. The 1972 marker bed and related facies changes are not found at the Beaver River mouth site BEA-1.

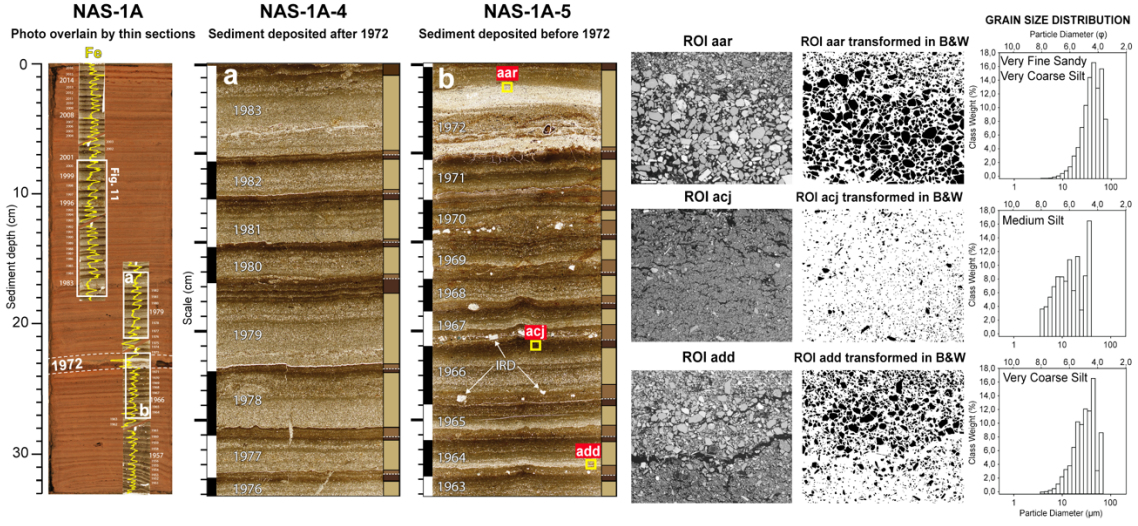

Figure 5. (Left) Photo of core NAS-1A overlain by thin-section image and Fe relative intensity profile (yellow lines). The 1972 marker layer is outlined by the white dashed lines. Thin-section images showing sedimentary structure of varves deposited (B) before and (A) after the 1972 marker bed. Varve boundaries are represented by the vertical black and white bars. Varve layers are delimited by the medium brown (early spring layer), pale brown (detrital layer) and dark brown (autumn and winter layer) bars. Typical Ice-Rafted Debris (IRD) are shown by the white arrows on the b panel. (Right) BSE images of three ROIs transformed in B&W and their associated particle size distribution (aar: the 1972 marker layer; acj: a typical autumn and winter layer; add: the base of a typical detrital layer) (see yellow squares on the b panel for ROIs location).

4.2 Varve chronology

The laminated sequences chronologies are consistent with the Cesium-137 main peaks corresponding to the highest atmospheric nuclear testing period (1963-1964 CE) (Appleby, 2001). Peaks are found at 14-14.5 cm (BEA-1) and 26.5-27 cm (NAS-1A) depth (Fig. 4) and perfectly match the lamination counts in both cores, confirming the varve assumption. The presence of the distinct 1972 marker layer at this chronostratigraphic position in the varve sequence which coincides with the occurrence of the Naskaupi River diversion that took place in April 1971 (see section 5.2 for details) supports the reliability of the constructed chronologies.

Independent varve chronologies were established from sediment cores BEA-1, NAS-1 and NAS-2 (Fig. 4). A total of 160 varves were counted at each site, covering the 1856-2016 period. The thickness and the good quality of the well-preserved varve structures allowed a robust age-model reproducible among cores to be constructed. Despite the distance between the coring sites (1 to 5 km) and the two different sediment sources (Naskaupi and Beaver River) (Fig. 1b), there is no varve count difference between the selected thick marker layers (A to M; Fig. 4) among cores. The few counting difficulties occur within varve years 1952-1953, 1935-1934, 1918-1919, as it contains ambiguous coarse non-annual intercalated sub-layers with intermediate clay cap that can be interpreted as one year of sedimentation. Both varve counts performed on thin-sections show a low overall counting error (±1.8%) which demonstrated the precision and accuracy of the varve sequences chronology. The age-depth models (Fig. 4, Box. 1) show changes in sediment accumulation rates (thickness) among cores in 1920 and 1972.

4.3 Thickness and particle size measurements

The TVTs from core BEA-1, NAS-1 and NAS-2 vary between 0.9 and 12.9 mm, with an average thickness of 4.09 mm (Fig. 6a, b, c, Supplements Fig. S1 and Tab. S1). The DLTs vary between 0.3 and 8.3 mm, with an average thickness of 1.9 mm (Fig. 6a, b, c, Supplements Fig. S2 and Tab. S2). There are significant strong positive correlations between TVT and DLT for each core ($r = 0.79$ to 0.91; $p < 0.01$). A step in the TVT is observable in the early 1920s at the three sites (Fig. 6a, b, c), especially in core NAS-2,

which recorded their highest values (12.9 mm) during the 1920-1972 period (Fig. 6c). Since the 1920s, there is a statistically significant decreasing trend in TVTs and DLTs in core BEA-1 (Fig. 6a). Thickness data from the three sites have been normalized and averaged to produce combined TVT and DLT series (Fig. 6d, e). From 1920 to 1972, combined TVT and DLT series show a statistically significant downward trend, despite an increase in years associated with high thickness values. Overall, TVT and DLT vary similarly in time between sites during the 1856-1971 period (Fig. 6d, e). However, after 1972, TVT and DLT series are more diverging. From 1972 to 2016, there is a statistically significant decreasing trend in TVT and DLT in cores NAS-2 (Fig. 6c), and the amplitude of their variability tends to diminish. For core NAS-1 (Fig. 6b), post-1971 period is associated with higher thickness values. Core NAS-1 has recorded a slight TVT and DLT decrease for the 1972-2016 period, but unlike the other cores, the variability tends to increase. The TVT and DLT are overall finer in the distal core NAS-2 compared to the more proximal core NAS-1 (Fig. 4, Box. 1, Supplements Tab. S1, S2).

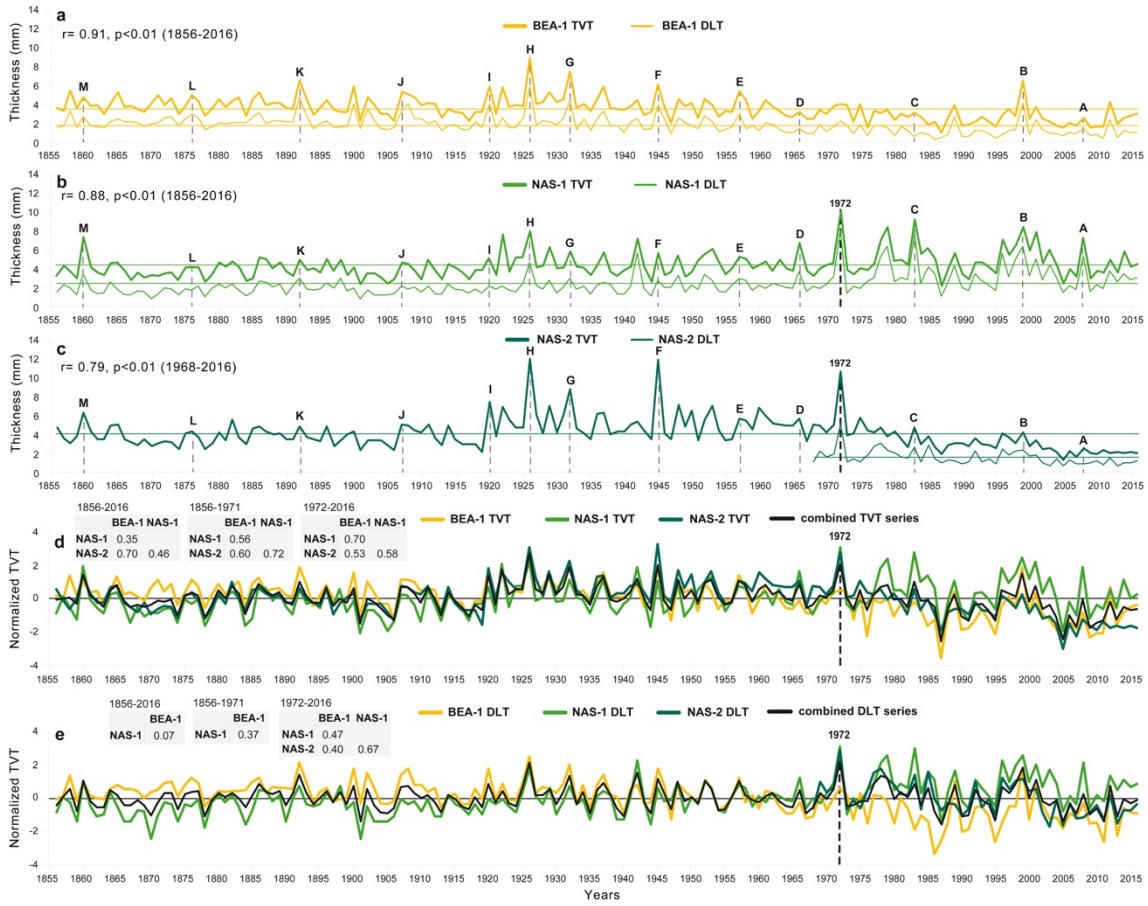

Figure 6. Total Varve Thickness (TVT; thick line) and Detrital Layer Thickness (DLT; thin line) time series of core (a) BEA-1, (b) NAS-1 and (c) NAS-2. Normalized (d) TVT and (e) DLT series and the combined series (mean of the normalized data from the 3 sites). Pearson correlation coefficients between TVT and DLT for the 1856-2016, 1856-1971 and 1973-2016 periods are shown. The selected marker layers are identified by letters A to M and the 1972 marker layer is outlined by the thick black dashed line.

The $P99D_0$ of cores BEA-1, NAS-1 and NAS-2 vary between 20 and 67.8 µm, with an average value of 34.3 µm (Fig. 7, Supplements Fig. S3 and Tab. S3). The grain size is finer in core NAS-2 compared to core NAS-1. Particle size data from the three sites have been normalized and averaged to produce combined $P99D_0$ series (Fig. 7c). The combined $P99D_0$ series show a slight coarsening trend towards the end of the 19th century. From 1900 to 1971, $P99D_0$ values are generally below average. The 1972 marker layer of core NAS-1 presented the maximum $P99D_0$ values (Fig. 7b). After 1972, there is an increase of $P99D_0$ values in core NAS-1, where a step is observable. Pre-1971 varves in core NAS-1 have a mean $P99D_0$ of 32,47 µm compared to 42,91 µm for the 1972-2016 period.

There is weak to moderate positive correlation between TVT and $P99D_0$ from a same core (BEA-1: $r = 0.41$ $p < 0.01$; NAS-1: $r = 0.52$ $p < 0.01$; NAS-2: $r = 0.27$, $p < 0.05$). The correlation between DLT with $P99D_0$ is stronger (BEA-1: $r = 0.49$ $p < 0.01$; NAS-1: $r = 0.65$ $p < 0.01$; NAS-2: $r = 0.49$, $p < 0.01$). Thick varves are more likely to have high grain size values. However, these correlations show that TVT, DLT and $P99D_0$ remain independent variables and can both reveal different hydrological information.

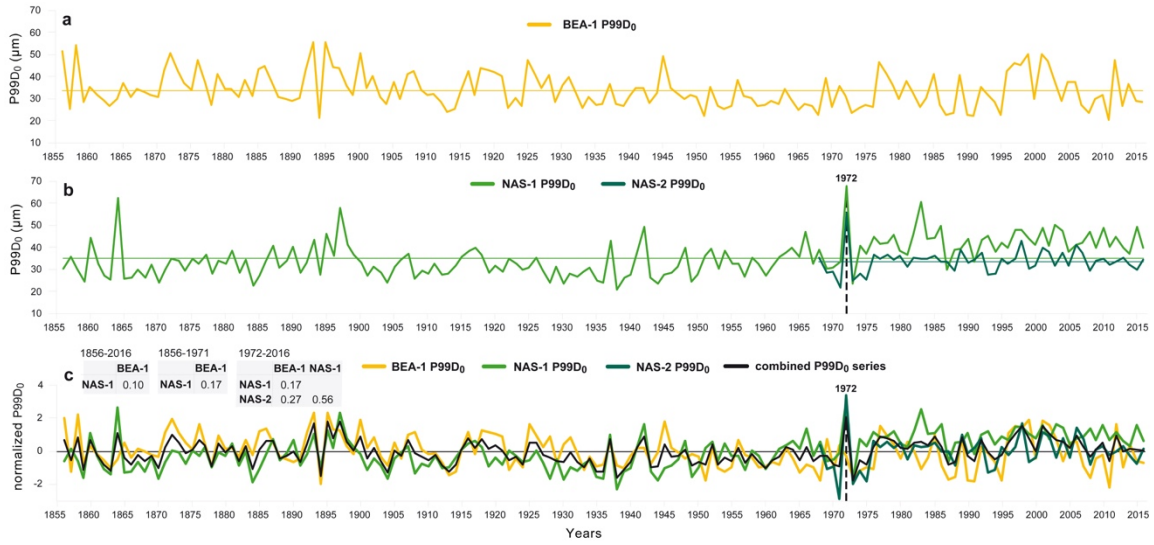

Figure 7. $P99D_0$ time series of cores (a) BEA-1, (b) NAS-1 (1856-2016) and NAS-2 (1968-2016). (c) Normalized $P99D_0$ series and the combined series (mean of the normalized data from the 3 sites). The 1972 marker layer is outlined by the black dashed line. Pearson correlation coefficients between $P99D_0$ series for the 1856-2016 and 1968-2016 periods are shown.

4.5 Relation between varve series and instrumental record

4.5.1 Naskaupi River

To examine how the physical parameters of the varves are related to local hydrology and to demonstrate their potential for hydrological reconstruction, sediment parameters (TVT, DLT and $P99D_0$) of each core were systematically compared to hydrological variables (Tab. 1). TVT, DLT and $P99D_0$ series from the three coring sites show significant positive correlations with the Q-mean and Q-max extracted from the Naskaupi River hydrometric station (03PB002) data on the 1978-2011 period (n=31) (Tab. 3). The TVT and DLT of cores BEA-1 and NAS-2 show stronger correlation with Q-mean, while TVT and DLT of cores NAS-1 have a better relation with Q-max. There is a significant negative correlation between $P99D_0$ of core NAS-1 and Q-max-Jd ($r = -0.38$) and Rise-Time ($r = -0.47$). Sediment parameters also present significant positive correlations with Q-Nival ($r = 0.32$

to 0.61) and Nb-days-SupQ80 (> 125 $m^3 \cdot s^{-1}$) (r = 0.44 to 0.62). Combined DLT and $P99D_0$ series (Fig. 6d, e; 7c) yields the strongest correlations in our dataset (r = 0.68 and 0.75; Tab. 3) and have been used to reconstruct Naskaupi River Q-mean and Q-max respectively (Fig. 8).

4.5.2 Labrador region

To determine if there is a regional hydrological signal in Labrador and whether the Grand Lake varved sedimentary sequence has recorded this signal, the Naskaupi River hydrological variables were compared with other Labrador hydrometric stations (Tab. 2). Despite specific local geomorphological and climatic conditions, strong similarities exist between observed mean daily discharges (Fig. 3c) and annual streamflow (Fig. 3d) recorded by hydrometric stations in Labrador for the 1978-2011 period. The shape of the five annual regimes shows similar characteristics (i.e. flood-timing, strength, duration, snowmelt and rainfall response). The instrumental Naskaupi River mean annual discharge series data show significant ($p < 0.01$, Supplements Tab. S5) positive correlations with other hydrometric stations (Ugjoktok: r = 0.84; Minipi: r = 0.70; Little Mecatina: r = 0.73; Eagle: r = 0.49). Hydrological conditions in the Naskaupi river region is thus representative of a broader region of Labrador. Therefore, the combined DLT series (without the NAS-1 1978-2016 period) has been used to reconstruct the Labrador region mean annual discharge series (Fig. 9).

Table 3. Matrix of correlation coefficients (Pearson r) of the hydrological variables defined in Tab. 1 with Total Varve Thickness (TVT), Detrital Layer Thickness (DLT) and particle size ($P99D_0$) on the instrumental period (1978-2011; n=31) for each core. Correlations between the hydrological variables and the combined TVT, DLT and $P99D_0$ series (normalized and averaged varve parameters of cores BEA, NAS-1 and NAS-2) are also present. Correlations in boldface are significant at $p < 0.05$ (Supplements Tab. S4). Correlations marked by an asterisk were used for the final Q-mean and Q-max reconstructions.

Sediment parameters	Hydrological variables of station 03PB002					
Core BEA-1	**Q-mean**	**Q-max**	**Q-max-Jd**	**Rise-Time**	**Nb-days-supQ80**	**Q-nival**
TVT	0,53	0,46	-0.19	-0.06	0.54	0.41
DLT	0,54	0,38	-0.01	0.22	0.44	0.32
$P99D_0$	0,56	0,56	-0.05	0.17	0.34	0.40
Core NAS-1	**Q-mean**	**Q-max**	**Q-max-Jd**	**Rise-Time**	**Nb-days-supQ80**	**Q-nival**
TVT	0.52	0,64	-0,31	-0,26	0,55	0,56
DLT	0.53	0,67	-0,31	-0,27	0,53	0,54
$P99D_0$	0.19	0,60	-0,38	-0,47	0,26	0,40
Core NAS-2	**Q-mean**	**Q-max**	**Q-max-Jd**	**Rise-Time**	**Nb-days-supQ80**	**Q-nival**
TVT	0,49	0,45	0,04	-0,24	0,56	0,47
DLT	0,62	0,57	0,07	-0,13	0,59	0,61
$P99D_0$	0,39	0,43	0,19	0,26	0,31	0,40
Combined series	**Q-mean**	**Q-max**	**Q-max-Jd**	**Rise-Time**	**Nb-days-supQ80**	**Q-nival**
TVT	0,56	0,58	-0,19	-0,20	0,60	0,53
DLT	0,68*	0,65	-0,11	-0,07	0,62	0,58
$P99D_0$	0,59	0,75*	-0,09	0,05	0,43	0,56

4.6 Hydrological reconstructions using varve parameters

4.6.1 Naskaupi River Q-mean and Q-max

The Naskaupi River mean and maximum annual discharges (Q-mean and Q-max) were reconstructed using DLT and $P99D_0$ series for the 1856–2016 period. The reconstructions were performed using single-core data, combined DLT and $P99D_0$ series and other combinations of core data, in order to propose the most relevant reconstructions (Supplements Fig. S4, S5). The observations and the reconstructed Q-mean and Q-max extracted from the different series over the 1978-2011 period are consistent. Despite differences, all reconstructions tested using different sources of sedimentological data generally share common interannual and longer-term variability.

Excluding the 1972-2016 measurements from NAS-1 from the combined series for reconstructions was also tested to remove the likely anthropogenic impact on sedimentation during this period. The combined DLT series without the 1972-2016 period presents a slightly better fit with the instrumental data (lowest RMSE and the most-significant and highest R^2, Supplements Tab. S6). The model calibrations based on a twofold cross-validation reveal that this DLT series has better overall predictive capacity to reconstructed Q-mean (Supplements Tab. S7). The 1972-2016 period of core NAS-1 was then excluded from the combined DLT series used to perform the best reconstruction of Naskaupi River Q-mean presented in Fig. 8a. However, significantly stronger calibration and validation statistical results were obtained by keeping this period in the combined $P99D_0$ series used to reconstruct Naskaupi River Q-max (Fig. 8b, Supplements Tab. S8, S9). The varve of year 1972 is considered as an outlier that originated from anthropogenic impacts, and thus was not included in all reconstructions.

The reconstructed Naskaupi River Q-mean from combined DLT series varies between 73 and 126 $m^3 \cdot s^{-1}$, with an average of 96 $m^3 \cdot s^{-1}$ (Fig. 8a), and remains relatively stable from 1856 to 1920, mainly near average. Several years with high Q-mean occurred during the 1920-1960 period. A statistically significant downward trend of the Q-mean is observed over the last 90 years. Recently, high Q-mean periods are observed from 1976 to 1985 and 1996 to 2002 and lower Q-mean periods from 1986 to 1995 and 2003 to 2016. The reconstructed Naskaupi Q-max from combined $P99D_0$ series varies between 192 and 681 $m^3 \cdot s^{-1}$, with an average of 426 $m^3 \cdot s^{-1}$ (Fig. 8b). There is a slight upward trend in Q-max at the end of the 19th century. The 1900-1971 period is characterized by a Q-max generally below average. Three periods of high Q-max are observed from 1887 to 1900, 1976 to 1986 and 1995 to 2008 (Fig. 8b).

4.6.2 Labrador region Q-mean

The consistency between combined DLT series and the observed Labrador region Q-mean series (Fig. 9), based on the discharge variability of five watersheds of different size and location, demonstrates that the Grand Lake varved sequence contains a regional signal. The best reconstruction of Labrador region mean annual discharges is the one performed using

the combined DLT series without the NAS-1 1972-2016 period. This reconstruction demonstrates the best predictive capacity (RE and CE must be > 0 to validate the model skills, Supplements Tab. S10, S11). The regional Q-mean reconstruction for the 1856–2016 period is presented in Fig. 9.

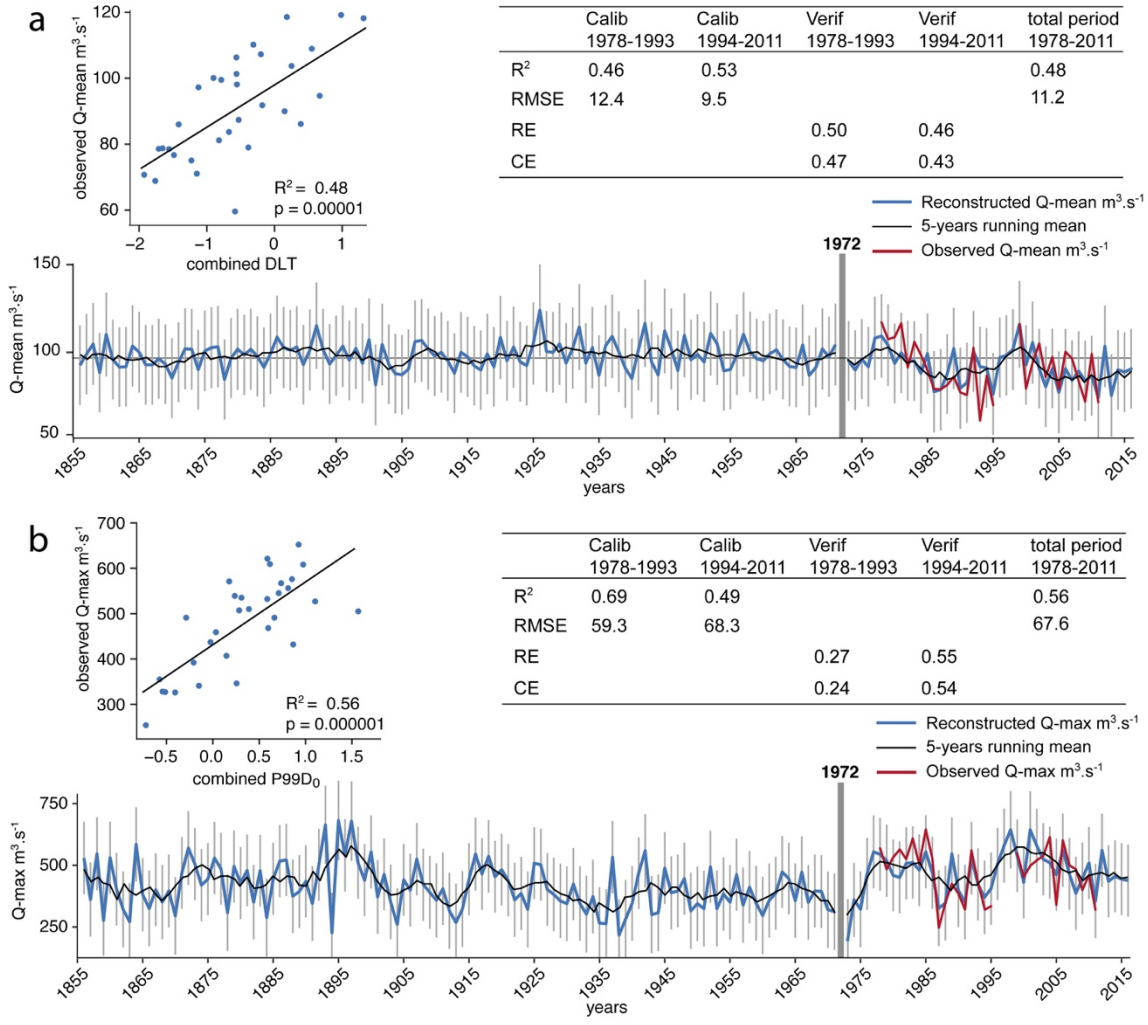

Figure 8. Naskaupi River (a) Q-mean and (b) Q-max reconstructed from combined DLT (Without the NAS-1 1978-2016 period) and P99D$_0$ series respectively, for the 1856–2016 period (blue line), with 5-year moving average (black line). Error bars represent the 95% confidence interval. Observed Q-mean and Q-max are also shown for the 1978-2011 period (red line).

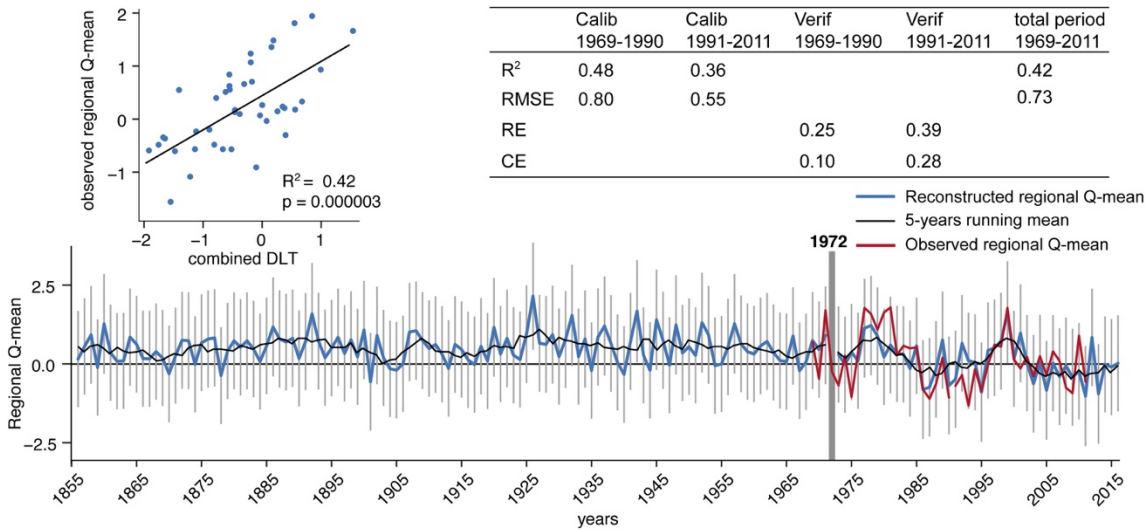

Figure 9. Labrador region Q-mean reconstructed from combined DLT series (without the NAS-1 1972-2016 period) for the 1856–2016 period (blue line), with 5-year moving average (black line). Error bars represent the 95% confidence interval. Observed Labrador region Q-mean series is also shown for the 1969-2011 period (red line).

4.7 Hydrological reconstruction using the rainfall-runoff modelling approach and comparison with the varved-based reconstruction

Naskaupi River Q-mean and Q-max (Fig. 8) were also reconstructed using the ANATEM rainfall-runoff modelling (Fig. 10). The independent modelling approach results show similarities with reconstructions based on varved series. The ANATEM reconstructions are statistically and positively correlated with the yearly time series obtained from combined DLT and $P99D_0$ series during the 1880-2011 period (Q-mean: $r = 0.41$; Q-max: $r = 0.22$; $n = 131$; $p < 0.01$). The reconstructed Q-mean and Q-max annual variabilities show similarities, especially during the 1973–2011 period (Q-mean: $r = 0.58$; Q-max: $r = 0.34$; $n = 43$ $p < 0.05$).

Q-mean reconstructions with both varve parameters and modelling are better correlated than the Q-max reconstructions. This may be due to the higher uncertainty related to the Q-max reconstruction with the modelling approach. Indeed, high flow modelling requires good reconstruction performances on several hydro-climatic processes (i.e., snow accumulation during the winter, timing of the snowmelt, spring precipitation). Moreover, the uncertainty of the hydrological reconstruction is less important on recent periods (>1950), due to the better quality of the geopotential height field reanalysis over recent decades, as more stations series are available and thus used in the reanalysis. The decrease

588 in the uncertainty related to reanalysis over time might explain the better correlation
589 between the two approaches for the recent period.

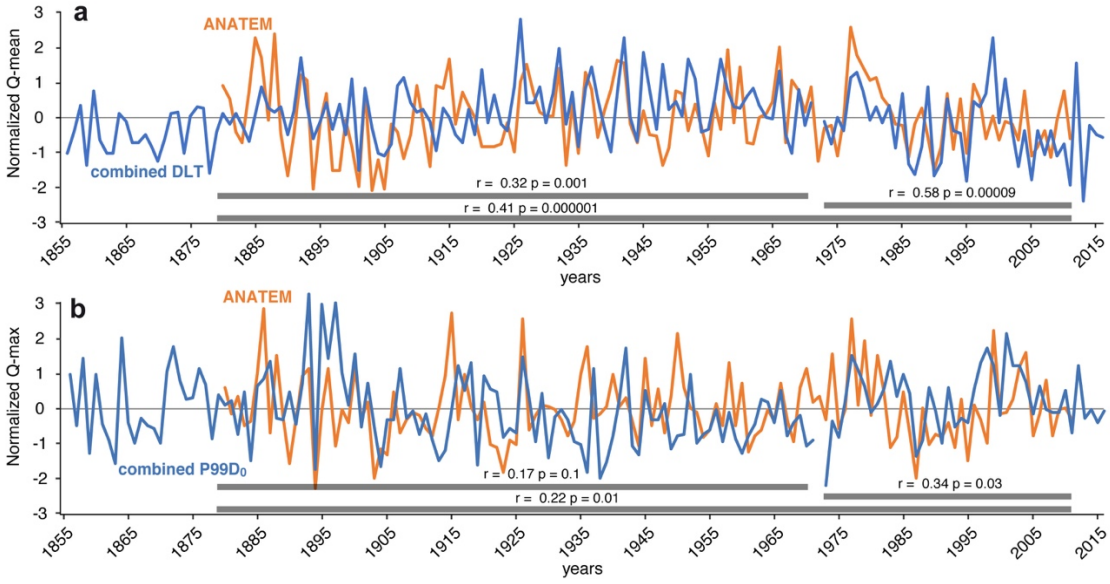

590

591 *Figure 10. Comparison between the Naskaupi River (a) Q-mean and (b) Q-max reconstruction using*
592 *combined Detrital Layer Thickness (DLT) (without the NAS-1 1972-2016 period) and P99D$_0$ series*
593 *respectively (blue line) and the rainfall-runoff modelling (orange line) for raw yearly data.*

5. Discussion

5.1 Grand Lake varve formation

Lakes containing well-defined and continuous varved sequences that allow the establishment of an internal chronology are rare in boreal regions. However, the great depth of Grand Lake, the availability of fine sediments in its watershed due to the glacial and postglacial history of the region (Trottier et al., 2020), as well as its important seasonal river inflow have favoured the formation and preservation of exquisite and thick varves. The seasonal streamflow regime plays a significant role in the annual cycle of sedimentation in Grand Lake and is responsible for the formation of the three distinct varve layers. Due to the thickness and the clarity of the varve structures, it is possible to infer the deposition mechanism for each layer and the season in which they were deposited.

The early spring layers are interpreted to be deposited during the river and lake ice break-up and disintegration period, when erosion and resuspension of fine-grained sediments are initiated but still low. Available Landsat-8 images of Grand Lake covering the 1983-2018 period (courtesy of the U.S. Geological Survey) shows that Grand Lake ice cover starts to melt at the Naskaupi and Beaver River mouths. This ice melting pattern creates open bays where drifting floating ice melts, thus depositing ice-rafted debris (Lamoureux 1999, 2004) as observed in the early spring layer facies. The overlying detrital layers are interpreted as flood-induced turbidites deposited at the lake bottom during the open-water season. High energy sediment-laden river flows produce hyperpycnal flows allowing silt and sand-size sediments to reach the cored sites (Cockburn and Lamoureux, 2008). The sharp contact boundary between the early spring layer and the detrital layer at the top part of the early spring layer supports the hypothesis that the detrital layers originate from underflows (Mangili et al., 2005). The sediment waves on the Naskaupi and Beaver river delta slopes (Trottier et al., 2020) (Fig. 1b, c) also indicate significant downstream sediment transport by supercritical density flows (Normandeau et al., 2016). The thick and grading upward basal part of the detrital layers are deposited during the high spring discharge period generated by snowmelt runoffs. The lack of erosion marks between the early spring layer and the detrital layer and the incorporation of rare cohesive sediment clasts within the detrital layer suggests that erosion of the underlying early spring layers occurs in more

proximal and energetic settings. Three observations justify the combination of varve measurements from the 3 coring sites : 1) the sedimentary processes inferred from the observation of thin-sections, the high resolution bathymetric and the sub-bottom surveys are similar; (2) the similarity of the varve facies and properties for each single year at the 3 different sites suggest a sedimentary pattern devoid of disturbances due to local factors; (3) Grains-size differences are too subtle to infer different sedimentary processes and environments. The upper part of varve structure in core NAS-1 show the most perceptible different after 1972 (see discussion below). In spring, river discharge reaches its annual peaks and sediment transport capacities that are then no longer reached during the rest of the summer and autumn (Fig. 2, 3c, 11). However, the presence of thin coarser intercalated sub-layers in the upper part of the detrital layer indicates that some rainfall events, as observed in Fig. 11 (i.e., 1983, 1987, 1992, 1999) also contribute to deposition of sediments in this layer. The overlying autumn and winter layer resulted from the settling and flocculation of fine particles in non-turbulent condition from fall through the onset of lake ice, forming a typical clay cap.

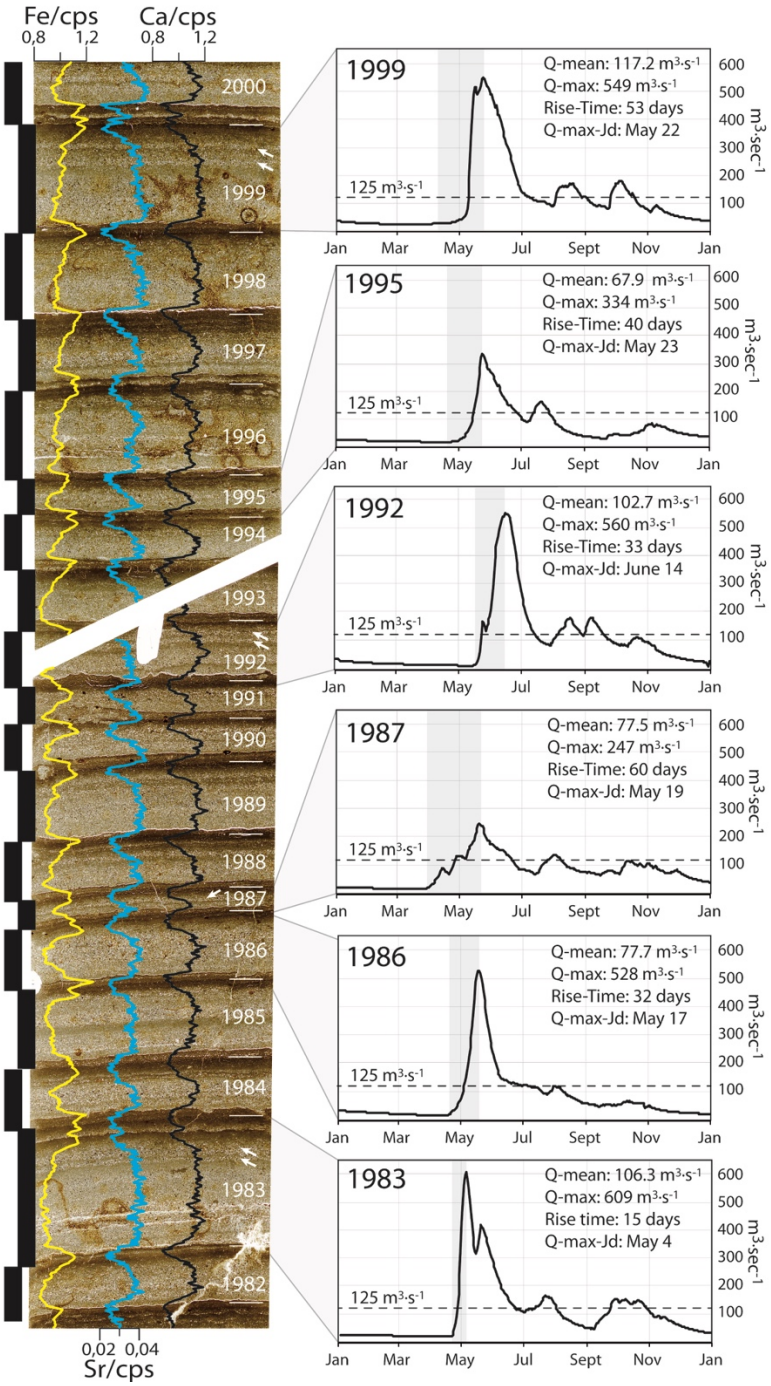

Figure 11. Qualitative comparison between NAS-1A varves from thin-sections (delimited by the black bars) with the hydrographs of the Naskaupi River. Observed annual Q-mean and Q-max as well as the timing and rise time of the peak spring discharge are shown. Black dotted lines represent the discharge threshold of ~125 $m^3 \cdot sec^{-1}$. (1999, 1992, 1986, 1983) Strong spring floods associated with thick coarse varves. (1995, 1987) Low spring floods associated with thin varves. (1999, 1992, 1987, 1983) Coarser intercalated sub-layers in the upper part of the detrital layer linked with summer and autumn high-discharge events. (1986) Strong spring flood with a low summer and autumn flow associated to a varve without substructure. Thin-sections are overlain by iron (Fe: yellow line), strontium (Sr: blue line), and calcium (Ca: black line) relative intensities. See Fig. 5 for thin-sections locations.

650 **5.2 Anthropogenic influences on recent sedimentation**

651 Anthropogenic environmental impacts on watersheds can be preserved in varved lake
652 sediments (Zolitschka et al., 2015; Saarni et al., 2016; Czymzik et al., 2018). Changes
653 observed in physical parameters of the varves deposited pre- and post-1971 at the NAS
654 sites suggest that the effect of the dyke system on the Naskaupi River sediment inputs is
655 perceptible in the Grand Lake varved sequence. The well-developed layers of varves
656 deposited prior to 1972 from sites NAS-1 (Fig. 6b) and NAS-2, and the similarity between
657 TVT and DLT values and variations among all sites over the 1856-1971 period (Fig. 6d)
658 indicate that before the Naskaupi River diversion, seasonal sedimentation cycles appeared
659 to have reached a relative state of equilibrium. The reduction of nearly half of the area of
660 the Naskaupi River watershed due to its diversion in April 1971, reduced the water inflows
661 and changed the base level of the downstream river system. The rapid base level fall must
662 have triggered modifications of the fluvial dynamics from late-spring to winter 1971 (i.e.,
663 channel incision, bank destabilization, and upstream knickpoint migration), likely
664 increasing the availability of sediments in the river system. The Naskaupi River
665 spring/summer/autumn flood(s) of 1972 have then remobilized and transported a large
666 amount of newly available floodplain sediments. This major sediment discharge plunged
667 in Grand Lake and extended as hyperpycnal flow in the axis of the Naskapi River
668 depositing a thick and coarse-grained turbidite following the lake bathymetry. This 1972
669 marker bed suggests that the Naskaupi River diversion had an impact on sedimentation at
670 sites NAS-1 and NAS-2.
671
672 The thin early spring layers free of ice-rafted debris in varve post-1971 of core NAS-1 (Fig.
673 5a, 11) and NAS-2 indicate the decrease of the capacity of early spring discharge to
674 transport fine sediments and its ability to float ice to Grand Lake (see section 4.1) due to
675 the reduction in water supplies caused by the Naskaupi River diversion. The increase in
676 thickness and particle size values of the detrital layers post-1971 in core NAS-1 (Fig. 5a,
677 6b, 7b, 11) suggest that the diversion has affected sedimentation at this site over time.
678 During the 1972-2016 period, the river floodplain morphology must have been in a re-
679 equilibration phase favourable to erosion, sediment transport, and deposition of thicker and
680 coarser detrital layers. Since the river diversion, detrital layers at NAS-1 site appears to

681 have become more sensitive to maximum spring discharges variations than mean annual
682 discharges. The sensitivity of the more proximal NAS-1 site to Naskaupi River extreme
683 discharges variability may partly explain why better results are obtained without the 1972-
684 2016 period to reconstruct Q-mean and by keeping this period to the Q-max reconstruction.
685 The negative correlation between $P99D_0$ of the core NAS-1 and the timing and rise time of
686 spring discharge (Table 3) also demonstrate reactivity to spring entrainment energy
687 conditions at this site. The distal NAS-2 site shows that post-1971, sedimentation seems to
688 have slightly lost sensitivity to river discharge, and that sediment input continued to decline
689 at the beginning of the deep lake basin. The increase in sediment input at the site NAS-1
690 after 1971, contrasts with the decrease in sediment input at the site NAS-2. This recent
691 difference in sedimentation between these two sites could be explained by the increased
692 availability of sediments for erosion in the floodplain, which would have favoured the
693 accumulation of additional sediments mainly on the front of the delta (NAS-1), while the
694 reduction in maximum discharges due to a smaller watershed would have resulted in a
695 decrease in the river's transport capacity to the site NAS-2.
696
697 It is indeed tempting to link the decrease of varve thickness in core NAS-2 over the 1972-
698 2016 period with the discharge reduction due to the river diversion. However, similarities
699 with core BEA-1, a site devoid of anthropogenic perturbations (unaffected by the Naskaupi
700 River diversion) which also shows a decline in varve thickness, suggest that this decrease
701 can potentially be due to natural hydro-climatic conditions. The observed Naskaupi River
702 Q-mean series also show a decrease on the 1978-2011 period. Indeed, because of the distant
703 location of site BEA-1 from the Nakaupi River mouth, the diversion is most likely not
704 responsible for the decrease of varve thickness in this sector. Moreover, it is quite unlikely
705 that the sedimentary input from the Naskaupi River contributed to sediment accumulation
706 at the mouth of the Beaver River. The absence of any traces of the 1972 marker bed at the
707 Beaver River mouth (BEA-1) supports this hypothesis. Furthermore, the thickness decrease
708 observed in BEA-1 began after ~1920 (Fig. 6a), which is before the 1971 diversion.
709
710 Anthropogenic modification of the Naskaupi River watershed makes it challenging to
711 discuss natural hydroclimate-related variations before and after 1971. Some caution should

712 be applied when comparing pre- to post 1972 reconstructions, given the changes in
713 watershed conditions that happened after the construction of the system of dykes. There is
714 no instrumental data available for the Naskaupi River watershed before 1971 to confirm
715 that the calibration model post-diversion (1978-2011) is similarly robust for the preceding
716 period. The river diversion affected the Naskaupi River sedimentation dynamics but did
717 not modify it drastically. Despite the observed post-diversion changes in varves' physical
718 parameters in cores NAS-1 and NAS-2, which are however moderate, the varves still
719 responded directly to variations in river discharge. In addition, the part of the watershed
720 that has been diverted is an area composed mainly of lakes, which are not very
721 hydrologically reactive.

722 **5.3 The hydrological signal in the varve record**

723 The significant correlations between continuous varve thickness and particle size
724 measurements with instrumental hydrological variables (Tab. 3) show that Grand Lake
725 varved sediments are reliable proxies to reconstruct past hydrologic conditions through
726 time at the annual to seasonal scale. The thick and/or coarse-grained varves correspond
727 well to years of high river discharges, whereas thin and/or fine-grained varves are related
728 with years of low discharge. Moreover, figure 11 clearly demonstrates how Grand Lake
729 varve record can be exploited to examine the interaction between meteorological
730 conditions and rivers discharge at an inter-seasonal scale, which is a temporal resolution
731 rarely obtained with natural proxies.
732
733 Data from the 3 sites were combined in order to better capture the regional hydrological
734 signal and to somehow attenuate the noise that is inherent from the analysis of a single core
735 in a very large lake. A single core will be more sensitive to local specificities and is
736 probably less representative of the entire hydrogram. The Beaver and the Naskaupi Rivers
737 have adjacent catchments that share the same climatological and geological characteristics,
738 while the Beaver River's catchment is devoid of anthropogenic modifications. The
739 combination of varve parameters from different coring sites with distinct sediment sources
740 (Fig. 1b) improved the correlations with local and regional hydrological variables (Tab. 3)
741 and thereby the reconstructions (Fig. 8, 9). By integrating the core BEA into the combined

742 data, it allows to capture the hydrological signal from a larger region (Nakaupi + Beaver
743 watersheds) and it helps to capture the natural hydrological signal in our combined series
744 used for reconstructions.
745
746 As demonstrated by previous studies on varved sediments, the use of both varve thickness
747 and particle size analysis allows for a more specific investigation of the range of
748 hydroclimate conditions recorded within varves (Francus et al., 2002; Cockburn and
749 Lamoureux, 2008; Lapointe et al., 2012). For Grand Lake, the combined DLT is found to
750 be the best proxy to reconstruct all hydrological events occurring throughout the year (Q-
751 mean). DLT series are better at predicting Q-mean because the early spring layers and
752 autumn and winter layers thickness are more variable and are included in the TVT
753 measurements. This variability can be linked to specific climatic and geomorphological
754 parameters such as the duration of ice cover on Grand Lake and the Naskaupi River ice
755 breakup processes which induce noise in the hydrologic signal contained in TVT series.
756 The combined $P99D_0$ yields the strongest correlation in our dataset (Tab. 3) and is the best
757 proxy to reconstruct maximum annual discharges (Q-max). This result is logical because
758 the peak discharge is controlling the competence of the river and consequently the size of
759 the particles that can be transported. Moreover, this indicator is not sensitive to sediment
760 compaction, which may affect other proxies based on thickness.
761
762 The significant positive correlations between varve physical parameters and Q-max and Q-
763 nival (Tab. 3) demonstrate that Grand Lake varve predominantly reflects spring discharge
764 conditions (e.g., Ojala and Alenius 2005; Lamoureux et al., 2006; Saarni et al., 2016;
765 Czymzik et al., 2018), which is the major component of the regional streamflow regimes
766 classified as nival (snowmelt-dominated) (Bonsal et al., 2019). In boreal regions, the
767 intensity and length of spring floods are controlled by the snow accumulation during winter
768 and by the temperature of the melting period (Hardy et al., 1996; Snowball et al., 1999;
769 Cockburn and Lamoureux, 2008; Ojala et al., 2013; Saarni et al., 2017). The negative
770 correlation between $P99D_0$ of the NAS-1 and the timing and rise time of spring discharge
771 suggests that early spring flows that increase rapidly are conducive conditions for high
772 entrainment energy and the deposition of coarser laminations on the distal part of the delta

slope (Fig. 11; site NAS-1). The erosion of detrital materials in early spring increases when the snowmelt runoffs occur on soils that are not yet stabilized and protected by vegetation (Ojala and Alenius 2005, Czymzik et al., 2018).

Intercalated sub-layers in the upper part of the detrital layer are interpreted to be produced by summer or fall rainfall events (Fig. 11). Yet, the significant positive correlations between varve thickness and Nb-days-SupQ80 suggests that a daily discharge of ~125 $m^3 \cdot s^{-1}$ represents an approximate threshold above which the deposition of coarse sediments in Grand Lake (detrital layers) is more likely to occur (Fig. 11) (e.g., Czymzik et al., 2010, Kämpf et la., 2014). According to the instrumental data (Fig. 2, 11), such a discharge can be generated during the summer/autumn period, confirming that rainfall events can indeed be triggering the deposition of thin intercalated sub-layers observed in the upper part of the detrital layers (Fig. 11).

The comparison between the Naskaupi River hydrological variables and other Labrador hydrometric stations (Fig. 3) show that a coherent regional hydrological pattern exists in the Labrador region. The performed regional Q-mean reconstitution and validation (Fig. 9) indicated that the Labrador region hydrologic signal is recorded in the Grand Lake varve sequence. The local and regional Q-mean reconstructed from the combined DLT series (without the NAS-1 1972-2016 period) suggest a statistically significant decreasing trend in mean annual discharge during the last 90 years. Naskaupi River Q-mean and Q-max reconstructions based on both varve series and rainfall-runoff modelling revealed high value periods from 1975 to 1985 and 1995 to 2005, and low values from 1986 to 1994 and 2006 to 2016 (Fig. 10). These results agree with the downward trend of the annual streamflow observed in eastern Canada during the 20th century in other studies and also with the reported higher river discharges from 1970 to 1979 and 1990 to 2007, and lower discharges from 1980 to 1989 (Zhang et al. 2001; Sveinsson et al., 2008; Jandhyala et al., 2009; Déry et al., 2009; Mortsch et al., 2015; Dinis et al., 2019).

In addition to providing a new high-quality varved record in eastern Canada, this research highlights the complementarity between palaeohydrological reconstructions extracted

804 from clastic varved sediments and rainfall-runoff modelling. Both methods independently
805 offer a similar, yet robust, centennial perspective on river discharge variability in an
806 important region for the economic and sustainable development of water resources in
807 Canada. Reconstructed long-term mean and maximum annual river discharges series
808 provide valuable quantitative information particularly for water supply management for
809 hydropower generation and the estimation of flood and drought hazards. The varved
810 sediment of Grand Lake also allows documenting the effect of dyke systems on the
811 downstream sediment transport dynamic into a watershed and its implication for
812 palaeohydrological reconstruction. Further investigation of the impacts of the Naskaupi
813 watershed reduction on sediment transport could help better refine these reconstructions.
814 Future work in Grand Lake should be directed towards the high-resolution analysis of long
815 sediment cores in order to produce longer reconstructions. The Grand Lake deeper varved
816 sequence potentially recorded the hydro-climatic variability that occurred during the Late
817 Holocene in region sensitive to the North Atlantic climate, allowing interesting prospects
818 into large-scale atmospheric and oceanic modes of variability.
819
820 **6. Conclusions**
821 The great depth of Grand Lake, the availability of fine sediments along its tributaries, and
822 its important seasonal river inflow have favoured the formation and preservation of fluvial
823 clastic laminated sediments. By using a new varved record in eastern Canada and a rainfall-
824 runoff modelling approach, this paper provides a better understanding of the recording of
825 hydrological conditions in large and deep boreal lakes and allows extending the discharge
826 series beyond the instrumental period as well as the spatial coverage of the rare annual
827 palaeohydrological proxies in North America. The key results of this study are:
828 • The annual character of the 160 years-long lamination sequence has been confirmed.
829 Each varve, composed of an early spring layer, a summer/autumn detrital layer and an
830 autumn and winter layer, represents one hydrological year.
831 • Grand Lake varve formation is mainly related to the largest hydrological event of the
832 year, the spring discharge, with contributions from summer and autumn rainfall events.
833 • Two hydrological parameters, the Naskaupi river Q-mean and Q-max annual
834 discharges, are robustly reconstructed from two independent varves physical

parameters, i.e., the detrital layer thickness (DLT) and grain size ($P99D_0$) respectively, over the 1856-2016 period. The reconstructed Q-mean series suggest that high Q-mean years occurred during the 1920-1960 period and a decrease in Q-mean takes place during the second half of the 20^{th} century.

- The same two hydrological parameters (Q-mean and Q-max), were also reconstructed using the ANATEM rainfall-runoff modelling. ANATEM discharges series show similarities with reconstructions based on the varved series, which support the reliability of the two independent reconstruction approaches.
- The statistically significant relation between combined DLT series and the observed Labrador region Q-mean series, extracted from five watersheds of different size and location, demonstrates that Grand Lake varved sequence can also be used as a proxy of regional river discharges conditions.
- The effects of Naskaupi River dyking in 1971 are clearly visible in the sedimentary record and affected sedimentary patterns afterwards. While this event makes the hydroclimatic reconstruction trickier, it remains that the outstanding quality of this varved sequence provides one of the best hydroclimatic reconstruction from a sedimentary record, with Pearson correlation coefficients up to $r = 0.75$.

Data availability

The dataset used in this study can be found at https://doi.org/10.5683/SP2/SAI39X. The Labrador hydrometric station data used in this study come from a Government of Canada website (https://wateroffice.ec.gc.ca).

Author contributions

This study is part of AGP's thesis under the supervision of PF and PL. AT and PL provided geophysical data (Fig. 1b, c) and useful information on the morpho-stratigraphical framework of Grand Lake. AGP and DF conducted the coring fieldtrip. AGP and PB collected instrumental data. PB calculated hydrological variables from instrumental data (Fig. 3) and performed the rainfall-runoff modelling. HD and AGP adapted the code used to establish the relationship between the varve parameters and the instrumental data and for the regression model. AGP performed most of the data analysis, wrote the manuscript and created the figures with contributions from PF and PB. All authors provided valuable feedback and contributed to the improvement of the manuscript.

Competing interests

The author Pierre Francus is a member of the editorial board of the journal.

Acknowledgments

This research was financially supported by NSERC-Ouranos-Hydro-Québec-Hydro-Manitoba through a CRD grant to P.F. and P.L. (PERSISTANCE project, É. Boucher et al.). This work was also supported by the FRQNT through a doctoral (B2X) research scholarship to A.G.P. and by the MOPGA Short Stay program grant at Université Côte d'Azur, Nice, France to A.G.P and P.B. A financial support for the fieldwork campaign at Grand Lake was provided by POLAR through the NSTP program to A.G.P. The authors are grateful to Arnaud De Coninck, David Deligny and Louis-Frédéric Daigle for their participation during fieldwork, laboratory and helpful discussions. We greatly thank Wanda and Dave Blake from North West River for their guiding experience and accommodation at Grand Lake. We thank the Labrador Institute at North West River for the use of their facility during fieldwork. We want to thank Stéphane Ferré from the Micro-Geoarchaeology Laboratory of the Center for Northern Studies (CEN) in Québec, QC,

885 Canada, for the production of the high-quality thin-sections used in this study. We would
886 also like to thank the three reviewers for their constructive review of this article. Finally,
887 many thanks to Monique Gagnon, Charles Smith and Clarence Gagnon for reviewing the
888 English of an earlier version of the manuscript.

References

Amann, B., Szidat, S., and Grosjean, M.: A millennial-long record of warm season precipitation and flood frequency for the North-western Alps inferred from varved lake sediments: implications for the future, Quaternary. Sci. Rev., 115, 89-100, https://doi.org/10.1016/j.quascirev.2015.03.002, 2015.

Anderson, T.: Rivers of Labrador, Canadian Special Publication of Fisheries and Aquatic Sciences 81, Ottawa, Ontario, 1985.

Appleby, P. and Oldfield, F.: The calculation of lead-210 dates assuming a constant rate of supply of unsupported 210Pb to the sediment, Catena, 5, 1-8, https://doi.org/10.1016/S0341-8162(78)80002-2, 1978.

Bégin, C., Gingras, M., Savard, M. M., Marion, J., Nicault, A., and Bégin, Y.: Assessing tree-ring carbon and oxygen stable isotopes for climate reconstruction in the Canadian northeastern boreal forest, Palaeogeography, Palaeoclimatology, Palaeoecology, 423, 91-101, https://doi.org/10.1016/j.palaeo.2015.01.021, 2015.

Bégin, Y., Nicault, A., Bégin, C., Savard, M. M., Arseneault, D., Berninger, F., Guiot, J., Boreux, J.-J., and Perreault, L.: Analyse dendrochronologique des variations passées du régime hydro climatique au complexe de la grande rivière dans le Nord du Québec, La Houille Blanche, 2007. 70-77, https://doi.org/10.1051/lhb:2007085, 2007.

Bonsal, B.R., Peters, D.L., Seglenieks, F., Rivera, A., and Berg, A.: Changes in freshwater availability across Canada; Chapter 6 in Canada's Changing Climate Report, (ed.) E. Bush and D.S. Lemmen; Government of Canada, Ottawa, Ontario, 2019.

Boucher, E., Nicault, A., Arseneault, D., Bégin, Y., and Karami, M. P.: Decadal Variations in Eastern Canada's Taiga Wood Biomass Production Forced by Ocean-Atmosphere Interactions, Sci. Rep. Uk., 7, 1-13, https://doi.org/10.1038/s41598-017-02580-9, 2017.

Boucher, É., Ouarda, T. B., Bégin, Y., and Nicault, A.: Spring flood reconstruction from continuous and discrete tree ring series, Water. Resour. Res., 47, https://doi.org/10.1029/2010WR010131, 2011.

Briffa, K., Jones, P., Pilcher, J., and Hughes, M.: Reconstructing summer temperatures in northern Fennoscandinavia back to AD 1700 using tree-ring data from Scots pine, Arct. Antartic. Alp. Research., 20, 385-394, https://doi.org/10.1080/00040851.1988.12002691, 1988.

Brigode, P., Brissette, F., Nicault, A., Perreault, L., Kuentz, A., Mathevet, T., and Gailhard, J.: Streamflow variability over the 1881–2011 period in northern Québec: comparison of hydrological reconstructions based on tree rings and geopotential height field reanalysis, Clim. Past, 12, 1785-1804, https://doi.org/10.5194/cp-12-1785-2016, 2016.

Cherry, J. E., Knapp, C., Trainor, S., Ray, A. J., Tedesche, M., and Walker, S.: Planning for climate change impacts on hydropower in the Far North, Hydrol. Earth Syst. Sci., 21, 133, https://doi:10.5194/hess-21-133-2017, 2017.

Cockburn, J. M. and Lamoureux, S. F.: Inflow and lake controls on short-term mass accumulation and sedimentary particle size in a High Arctic lake: implications for interpreting varved lacustrine sedimentary records, J. Paleolimnol., 40, 923-942, https://doi.org/10.1007/s10933-008-9207-5, 2008.

Collins, M., Knutti, R., Arblaster, J., Dufresne, J-L., Fichefet, T., Friedlingstein, P., Gao, X., Gutowski, W. J., Johns, T., Krinner, G., Shongwe, M., Tebaldi, C., Weaver, A. J., Wehner, M. F., Allen, M. R., Andrews, T., Beyerle, U., Bitz, C. M., Bony, S., & Booth, B. B. B.: Long-term climate change: projections, commitments and irreversibility, In: Climate Change 2013 - The Physical Science Basis, Contribution of Working Group I to the Fifth Assessment Report of the Intergovernmental Panel on Climate Change, Intergovernmental Panel on Climate Change, Cambridge University Press, 1029-1136, 2013.

Compo, G. P., Whitaker, J. S., Sardeshmukh, P. D., Matsui, N., Allan, R. J., Yin, X., Gleason, B. E., Vose, R. S., Rutledge, G., and Bessemoulin, P.: The twentieth century reanalysis project, Q J R Meteorol Soc, 137, 1-28, https://doi.org/10.1002/qj.776, 2011.

Cook, E. R., Meko, D. M., Stahle, D. W., and Cleaveland, M. K.: Drought reconstructions for the continental United States, J. Clim., 12, 1145-1162, https://doi.org/10.1175/1520-0442(1999)012%3C1145:DRFTCU%3E2.0.CO;2, 1999.

Coron, L., Thirel, G., Delaigue, O., Perrin, C., and Andréassian, V.: The suite of lumped GR hydrological models in an R package, Environmental Modelling & Software, 94, 166-171, https://doi.org/10.1016/j.envsoft.2017.05.002, 2017.

Croudace, I. W., Rindby, A., and Rothwell, R. G.: ITRAX: description and evaluation of a new multi-function X-ray core scanner, Geological Society, London, Special Publications, 267, 51-63, https://doi.org/10.1144/GSL.SP.2006.267.01.04, 2006.

Cuven, S., Francus, P., and Lamoureux, S.: Mid to Late Holocene hydroclimatic and geochemical records from the varved sediments of East Lake, Cape Bounty, Canadian High

969 Arctic, Quaternary. Sci. Rev., 30, 2651-2665,
970 https://doi.org/10.1016/j.quascirev.2011.05.019, 2011.
971
972 Cuven, S., Francus, P., and Lamoureux, S. F.: Estimation of grain size variability with
973 micro X-ray fluorescence in laminated lacustrine sediments, Cape Bounty, Canadian High
974 Arctic, J. Paleolimnol., 44, 803-817, https://doi.org/10.1007/s10933-010-9453-1, 2010.
975
976 Czymzik, M., Dulski, P., Plessen, B., Von Grafenstein, U., Naumann, R., and Brauer, A.:
977 A 450 year record of spring-summer flood layers in annually laminated sediments from
978 Lake Ammersee (southern Germany), Water. Resour. Res., 46,
979 https://doi.org/10.1029/2009WR008360, 2010.
980
981 Czymzik, M., Haltia, E., Saarni, S., Saarinen, T., and Brauer, A.: Differential North
982 Atlantic control of winter hydroclimate in late Holocene varved sediments of Lake
983 Kortejärvi, eastern Finland, Boreas, 47, 926-937, https://doi.org/10.1111/bor.12315, 2018.
984
985 D'Arrigo, R., Buckley, B., Kaplan, S., and Woollett, J.: Interannual to multidecadal modes
986 of Labrador climate variability inferred from tree rings, Clim. Dynam., 20, 219-228,
987 https://doi.org/10.1007/s00382-002-0275-3, 2003.
988
989 Déry, S. J. and Wood, E. F.: Decreasing river discharge in northern Canada, Geophys. Res.
990 Lett., 32, https://doi.org/10.1029/2005GL022845, 2005.
991
992 Dinis, L., Bégin, C., Savard, M. M., Marion, J., Brigode, P., and Alvarez, C.: Tree-ring
993 stable isotopes for regional discharge reconstruction in eastern Labrador and
994 teleconnection with the Arctic Oscillation, Clim. Dynam., 53, 3625-3640,
995 https://doi.org/10.1007/s00382-019-04731-2, 2019.
996
997 Fitzhugh, W.: Environmental Approaches to the Prehistory of the North, Journal of the
998 Washington Academy of Sciences, 1973. 39-53, 1973.
999
1000 Francus, P.: An image-analysis technique to measure grain-size variation in thin sections
1001 of soft clastic sediments, Sedimentary Geology, 121, 289-298,
1002 https://doi.org/10.1016/S0037-0738(98)00078-5, 1998.
1003
1004 Francus, P., Bradley, R. S., Abbott, M. B., Patridge, W., and Keimig, F.: Paleoclimate
1005 studies of minerogenic sediments using annually resolved textural parameters, Geophys.
1006 Res. Lett., 29, 59-51-59-54, https://doi.org/10.1029/2002GL015082, 2002.
1007

1008 Francus, P. and Cosby, C. A.: Sub-sampling unconsolidated sediments: A solution for the
1009 preparation of undistrubed thin-sections from clay-rich sediments, J. Paleolimnol, 26, 323-
1010 326, https://doi.org/10.1023/A:1017572602692, 2001.
1011
1012 Francus, P. and Karabanov, E.: A computer-assisted thin-section study of Lake Baikal
1013 sediments: a tool for understanding sedimentary processes and deciphering their climatic
1014 signal, Int. J. Earth. Sci., 89, 260-267, https://doi.org/10.1007/s005319900064, 2000.
1015
1016 Francus, P., Keimig, F., and Besonen, M.: An algorithm to aid varve counting and
1017 measurement from thin-sections, Journal of Paleolimnology, 28, 283-286,
1018 https://doi.org/10.1023/A:1021624415920, 2002.
1019
1020 Francus, P. and Nobert, P.: An integrated computer system to acquire, process, measure
1021 and store images of laminated sediments, In 4th International limnogeology congress,
1022 Barcelona, July, 2007.
1023
1024 Fulton, R. J. and Ferguson, J.: Surficial Geology Cartwright: Labrador, Newfoundland,
1025 Commission, Department of Energy, Mines and Resources, 1986.
1026
1027 Gilbert, R. and Desloges, J. R.: Late glacial and Holocene sedimentary environments of
1028 Quesnel Lake, British Columbia, Geomorphology, 179, 186-196,
1029 https://doi.org/10.1016/j.geomorph.2012.08.010, 2012.
1030
1031 Gupta, H. V., Kling, H., Yilmaz, K. K., and Martinez, G. F.: Decomposition of the mean
1032 squared error and NSE performance criteria: Implications for improving hydrological
1033 modelling, J. Hydrol., 377, 80-91, https://doi.org/10.1016/j.jhydrol.2009.08.003, 2009.
1034
1035 Hardy, D. R., Bradley, R. S., and Zolitschka, B.: The climatic signal in varved sediments
1036 from Lake C2, northern Ellesmere Island, Canada, J. Paleolimnol., 16, 227-238,
1037 https://doi.org/10.1007/BF00176938, 1996.
1038
1039 Heideman, M., Menounos, B., and Clague, J. J.: An 825-year long varve record from
1040 Lillooet Lake, British Columbia, and its potential as a flood proxy, Quaternary. Sci. Rev.,
1041 126, 158-174, https://doi.org/10.1016/j.quascirev.2015.08.017, 2015.
1042
1043 Jandhyala, V. K., Liu, P., and Fotopoulos, S. B.: River stream flows in the northern Québec
1044 Labrador region: A multivariate change point analysis via maximum likelihood, Water.
1045 Resour. Res., 45, https://doi.org/10.1029/2007WR006499, 2009.
1046
1047 Kämpf, L., Brauer, A., Swierczynski, T., Czymzik, M., Mueller, P., and Dulski, P.:
1048 Processes of flood-triggered detrital layer deposition in the varved Lake Mondsee sediment

record revealed by a dual calibration approach, Journal of Quaternary Science, 29, 475-486, https://doi.org/10.1002/jqs.2721, 2014.

Kaufman, C. A., Lamoureux, S. F., and Kaufman, D. S.: Long-term river discharge and multidecadal climate variability inferred from varved sediments, southwest Alaska, Quat. Res., 76, 1-9, https://doi.org/10.1016/j.yqres.2011.04.005, 2011.

Kuentz, A., Mathevet, T., Gailhard, J., and Hingray, B.: Building long-term and high spatio-temporal resolution precipitation and air temperature reanalyses by mixing local observations and global atmospheric reanalyses: the ANATEM model, Hydrol. Earth Syst. Sci., 19, 2717-2736, https://doi.org/10.5194/hess-19-2717-2015, 2015.

Kylander, M. E., Ampel, L., Wohlfarth, B., and Veres, D.: High-resolution X-ray fluorescence core scanning analysis of Les Echets (France) sedimentary sequence: new insights from chemical proxies, J. Quat. Sci., 26, 109-117, https://doi.org/10.1002/jqs.1438, 2011.

Lamoureux, S.: Five centuries of interannual sediment yield and rainfall-induced erosion in the Canadian High Arctic recorded in lacustrine varves, Water. Resour. Res., 36, 309-318, https://doi.org/10.1029/1999WR900271, 2000.

Lamoureux, S. F.: Embedding unfrozen lake sediments for thin section preparation, J. Paleolimnol., 10, 141-146, https://doi.org/10.1007/BF00682510, 1994.

Lamoureux, S. F., Stewart, K. A., Forbes, A. C., and Fortin, D.: Multidecadal variations and decline in spring discharge in the Canadian middle Arctic since 1550 AD, Geophys. Res. Lett., 33, https://doi.org/10.1029/2005GL024942, 2006.

Lapointe, F., Francus, P., Lamoureux, S. F., Saïd, M., and Cuven, S.: 1750 years of large rainfall events inferred from particle size at East Lake, Cape Bounty, Melville Island, Canada, J. paleolimnol., 48, 159-173, https://doi.org/10.1007/s10933-012-9611-8, 2012.

Linderholm, H. W., Nicolle, M., Francus, P., Gajewski, K., Helama, S., Korhola, A., Solomina, O., Yu, Z., Zhang, P., D'Andrea, W. J., Debret, M., Divine, D. V., Gunnarson, B. E., Loader, N. J., Massei, N., Seftigen, K., Thomas, E. K., Werner, J., Andersson, S., Berntsson, A., Luoto, T. P., Nevalainen, L., Saarni, S., and Väliranta, M.: Arctic hydroclimate variability during the last 2000 years: current understanding and research challenges, Clim. Past, 14, 473–514, https://doi.org/10.5194/cp-14-473-2018, 2018.

Ljungqvist, F. C., Krusic, P. J., Sundqvist, H. S., Zorita, E., Brattström, G., and Frank, D.: Northern Hemisphere hydroclimate variability over the past twelve centuries, Nature, 532, 94-98, https://doi.org/10.1038/nature17418, 2016.

Mangili, C., Brauer, A., Moscariello, A., and Naumann, R.: Microfacies of detrital event layers deposited in Quaternary varved lake sediments of the Piànico-Sèllere Basin (northern Italy), Sedimentology, 52, 927-943, https://doi.org/10.1111/j.1365-3091.2005.00717.x, 2005.

Mortsch, L., Cohen, S., and Koshida, G.: Climate and water availability indicators in Canada: Challenges and a way forward. Part II–Historic trends, Can. Water Resour. J., 40, 146-159, https://doi.org/10.1080/07011784.2015.1006024, 2015.

Naulier, M., Savard, M. M., Bégin, C., Gennaretti, F., Marion, J., Nicault, A., and Bégin, Y.: A millennial summer temperature reconstruction for northeastern Canada using oxygen isotopes in subfossil trees, Clim. Past, 11, 1153-1164, https://doi.org/10.5194/cp-11-1153-2015, 2015.

Nicault, A., Boucher, E., Bégin, C., Guiot, J., Marion, J., Perreault, L., Roy, R., Savard, M. M., and Bégin, Y.: Hydrological reconstruction from tree-ring multi-proxies over the last two centuries at the Caniapiscau Reservoir, northern Québec, Canada, J. Hydrol., 513, 435-445, https://doi.org/10.1016/j.jhydrol.2014.03.054, 2014.

Normandeau, A., Lajeunesse, P., Poiré, A. G., and Francus, P.: Morphological expression of bedforms formed by supercritical sediment density flows on four fjord-lake deltas of the south-eastern Canadian Shield (Eastern Canada), Sedimentology, 63, 2106-2129, https://doi.org/10.1111/sed.12298, 2016.

Notzl, L., Greene, R., and Riley, J.: Labrador Nature Atlas. Vol. II. Ecozones, Ecoregions, and Ecodistricts, Nature Conservancy of Canada and Province of Newfoundland and Labrador, Toronto, ON, Canada, 2013.

Ojala, A. E. and Alenius, T.: 10 000 years of interannual sedimentation recorded in the Lake Nautajärvi (Finland) clastic–organic varves, Palaeogeography, Palaeoclimatology, Palaeoecology, 219, 285-302, https://doi.org/10.1016/j.palaeo.2005.01.002, 2005.

Ojala, A. E., Kosonen, E., Weckström, J., Korkonen, S., and Korhola, A.: Seasonal formation of clastic-biogenic varves: the potential for palaeoenvironmental interpretations, GFF, 135, 237-247, https://doi.org/10.1080/11035897.2013.801925, 2013.

Oudin, L., Hervieu, F., Michel, C., Perrin, C., Andréassian, V., Anctil, F., and Loumagne, C.: Which potential evapotranspiration input for a lumped rainfall–runoff model?: Part 2—Towards a simple and efficient potential evapotranspiration model for rainfall–runoff modelling, J. Hydrol., 303, 290-306, https://doi.org/10.1016/j.jhydrol.2004.08.026, 2005.

Perrin, C., Michel, C., and Andréassian, V.: Improvement of a parsimonious model for streamflow simulation, J. Hydrol., 279, 275-289, https://doi.org/10.1016/S0022-1694(03)00225-7, 2003.

Rohde, R., Muller, R., Jacobsen, R., Muller, E., Perlmutter, S., Rosenfeld, A., Wurtele, J., Groom, D., and Wickham, C.: A New Estimate of the Average Earth Surface Land Temperature Spanning 1753 to 2011, Geoinfor. Geostat.: An Overview 1: 1, of, 7, 2, http://dx.doi.org/10.4172/2327-4581.1000101, 2013.

Saarni, S., Lensu, A., Tammelin, M., Haltia, E., and Saarinen, T.: Winter climate signal in boreal clastic-biogenic varves: a comprehensive analysis of three varved records from 1890 to 1990 AD with meteorological and hydrological data from Eastern Finland, GFF, 139, 314-326, https://doi.org/10.1080/11035897.2017.1389984, 2017.

Saarni, S., Saarinen, T., and Dulski, P.: Between the North Atlantic Oscillation and the Siberian High: A 4000-year snow accumulation history inferred from varved lake sediments in Finland, Holocene, 26, 423-431, https://doi.org/10.1177/0959683615609747, 2016.

Schillereff, D. N., Chiverrell, R. C., Macdonald, N., and Hooke, J. M.: Flood stratigraphies in lake sediments: A review, Earth-Sci. Rev., 135, 17-37, https://doi.org/10.1016/j.earscirev.2014.03.011, 2014.

Seiller, G., Anctil, F., and Perrin, C.: Multimodel evaluation of twenty lumped hydrological models under contrasted climate conditions, Hydrol. Earth Syst. Sci., https://dx.doi.org/10.5194/hess-1116-1171-2012, 2012.

Snowball, I., Sandgren, P., and Petterson, G.: The mineral magnetic properties of an annually laminated Holocene lake-sediment sequence in northern Sweden, Holocene, 9, 353-362, https://doi.org/10.1191/095968399670520633, 1999.

St-Onge, G., Mulder, T., Francus, P., and Long, B.: Chapter two continuous physical properties of cored marine sediments, Developments in marine geology, 1, 63-98, https://doi.org/10.1016/S1572-5480(07)01007-X, 2007.

Stocker, T. F., Qin, D., Plattner, G.-K., Tignor, M. M., Allen, S. K., Boschung, J., Nauels, A., Xia, Y., Bex, V., and Midgley, P. M.: Climate change 2013: the physical science basis. Contribution of working group I to the fifth assessment report of IPCC the intergovernmental panel on climate change. Cambridge University Press, https://dx.doi.org/10.1017/CBO9781107415324, 2014.

Sturm, M.: Origin and composition of clastic varves, In: Schlüchter, C. (Ed.), Moraines and Varves: Origin, Genesis, Classification. A.A. Balkema, Rotterdam, The Netherlands, 281-285, https://www.worldcat.org/title/moraines-and-varves-origin-genesis-classification/oclc/5542145, 1979.

Sveinsson, O. G., Lall, U., Fortin, V., Perrault, L., Gaudet, J., Zebiak, S., and Kushnir, Y.: Forecasting spring reservoir inflows in Churchill Falls basin in Quebec, Canada, J. Hydrol. Eng., 13, 426-437, https://dx.doi.org/10.1061/(Asce)1084-0699(2008)13:6(426), 2008.

R Core Team: R: A Language and Environment for Statistical Computing, R Foundation for Statistical Computing, Vienna, Austria, http://www.R-project.org/, 2019.

Tomkins, J. D., Lamoureux, S. F., Antoniades, D., and Vincent, W. F.: Autumn snowfall and hydroclimatic variability during the past millennium inferred from the varved sediments of meromictic Lake A, northern Ellesmere Island, Canada, Quat. Res., 74, 188-198, https://doi.org/10.1016/j.yqres.2010.06.005, 2010.

Trottier, A. P., Lajeunesse, P., Gagnon-Poiré, A., and Francus, P.: Morphological signatures of deglaciation and postglacial sedimentary processes in a deep fjord-lake (Grand Lake, Labrador), Earth Surf. Proc. Land., 45, 928-947, https://doi.org/10.1002/esp.4786, 2020.

Valéry, A., Andréassian, V., and Perrin, C.: 'As simple as possible but not simpler': What is useful in a temperature-based snow-accounting routine? Part 1–Comparison of six snow accounting routines on 380 catchments, J. Hydrol, 517, 1166-1175, https://doi.org/10.1016/j.jhydrol.2014.04.059, 2014a.

Valéry, A., Andréassian, V., and Perrin, C.: 'As simple as possible but not simpler': What is useful in a temperature-based snow-accounting routine? Part 2–Sensitivity analysis of the Cemaneige snow accounting routine on 380 catchments, J. Hydrol., 517, 1176-1187, https://doi.org/10.1016/j.jhydrol.2014.04.058, 2014b.

Viau, A. E. and Gajewski, K.: Reconstructing millennial-scale, regional paleoclimates of boreal Canada during the Holocene, J. Clim., 22, 316-330, https://doi.org/10.1175/2008JCLI2342.1, 2009.

Zang, C. and Biondi, F.: treeclim: an R package for the numerical calibration of proxy-climate relationships, Ecography, 38, 431-436, 10.1111/ecog.01335, 2015.

Zhang, X., Harvey, K. D., Hogg, W., and Yuzyk, T. R.: Trends in Canadian streamflow, Water Resour. Res., 37, 987-998, https://doi.org/10.1029/2000WR900357, 2001.

Zolitschka, B., Francus, P., Ojala, A. E., and Schimmelmann, A.: Varves in lake sediments–a review, Quaternary. Sci. Rev., 117, 1-41, https://doi.org/10.1016/j.quascirev.2015.03.019, 2015.